Supported Noyori-Ikariya catalysts for asymmetric transfer hydrogenations and related tandem reactions

Han Peng, Vincent Ritleng, Christophe Michon

Supported Noyori-Ikariya catalysts for asymmetric transfer hydrogenations and related tandem reactions

Han Peng,[a] Vincent Ritleng,[a] Christophe Michon*[a]

a) Université de Strasbourg, Université de Haute-Alsace, Ecole européenne de Chimie, Polymères et Matériaux, CNRS, LIMA, UMR 7042, 25 rue Becquerel, 67087 Strasbourg, France.
Email: cmichon@unistra.fr

Dedicated to Dr Francine Agbossou-Niedercorn at the occasion of her retirement

Abstract. Following the impressive rise of homogeneous ruthenium-based bifunctional catalysts in asymmetric transfer hydrogenation, Noyori-Ikariya catalysts have gradually been supported on a plethora of materials like silicas, polymers, ionic liquids or micelles for economic, environmental and societal reasons. These supported catalysts have allowed asymmetric transfer hydrogenation of carbonyl derivatives and imines with high activities and enantioselectivities. Furthermore, they have been combined with other supported organometallic or organic catalysts to perform effectively tandem reactions combining transfer hydrogenation with Sonogashira or Suzuki cross-couplings, aza-Michael reaction, alkyne hydration, lactonisation, oxysulfonylation or oxidation. This article reviews over the past 7 years the development of supported Noyori-Ikariya catalysts based on ruthenium, rhodium and iridium for asymmetric transfer hydrogenation of various CO and CN double bonds and related tandem reactions through the use of an additional supported organometallic or organic catalyst. It highlights and discusses the synthesis, reactivity and performances of these new bifunctional catalysts, as well as their recycling.

Keywords: transfer hydrogenation, tandem reactions, asymmetric catalysis, supported catalysis

Table of content

Abreviations

AH: asymmetric hydrogenation

ATH: asymmetric transfer hydrogenation

cat: catalyst

CD: cyclodextrin

Cp*: pentamethylcyclopentadienyl

COD: cyclooctadiene

conv: conversion

DABCO: 1,4-diazabicyclo[2.2.2]octane

de: diastereomeric excess

DKR: dynamic kinetic resolution

DPEN: diphenylethylenediamine

dr: diastereomeric ratio

ee: enantiomeric excess

ICP-AES: inductively coupled plasma – atomic emission spectroscopy

IL: ionic liquid

IPr: 1,3-(2,6-diisopropylphenyl)imidazol-2-ylidene

NMR: Nuclear Magnetic Resonance

PEG: polyethylene glycol

TEM: transmission electron microscopy

TEMPO: 2,2,6,6-tetramethylpiperidine-1-oxyl

THF: tetrahydrofurane

TOF: turnover frequency

TON: turnover number

Tres: Time of residence

TsDPEN: 1,2- diphenylethyl-4-methylbenzenesulfonamidato

1. Introduction

Asymmetric hydrogenation is an effective and useful synthetic methodology that provides a high degree of stereocontrol for the preparation of optically pure fine chemicals such as agrochemicals, fragrances and pharmaceuticals. Asymmetric hydrogenations (AH) of alkenes and ketones have been developed in homogeneous conditions using chiral organometallic catalysts in the presence of hydrogen gas and have allowed single enantiomer syntheses for the preparation of advanced chemicals at industrial scales [1-13]. Initially, most of the catalysts involved were based on rhodium(I) and required the presence of functional groups on the substrates in order to coordinate the metal and enable hydrogenation of the unsaturated bonds in highly efficient and selective manner [14]. Though the developed catalysts hydrogenated effectively and selectively various alkenes, they remained almost inert toward ketones [15].

In 1995, Noyori and co-workers found the combination of a ruthenium precursor, BINAP ligand, a chiral diamine and KOH allowed the hydrogenation of simple aromatic ketones with high enantioselectivity in the presence of isopropanol as a hydrogen donor [16-17]. Shortly after, the same group reported a further significant achievement with the use of η^6-arene ruthenium catalysts with N-sulfonylated 1,2-diamines or amino-alcohol as chiral ligands, for the highly efficient asymmetric transfer hydrogenation (ATH) of ketones [18-20]. The AH[15,21] and ATH[22-23] of ketones both involved a metal-ligand bifunctional mechanism [21,24-26] that was established through kinetic studies, isotopic labelling [22,27-28] and theoretical calculations [28-30].

Afterwards, the concept of bifunctional catalysis has been further applied in C–H, C–C, C–N, and CO formation[31-38]. In ATH, 2-propanol or formic acid, i.e. two cheap, non-toxic and environmentally safe hydrogen sources, are commonly used without the need of pressurised reactors. However, the thermodynamic reversibility of the ATH reaction while using 2-propanol can lead to limited conversions and to a gradual decrease of the enantiomeric purity of the targeted chiral alcohol. The use of formic acid can help overcoming such a drawback and favor full conversions through removal of the released CO_2. Therefore, the Noyori half-sandwich bifunctional catalysts offer a great potential in enantioselective synthesis allowing effective ATH with hydrogen sources like 2-propanol or an azeotropic mixture of formic acid. As a result, these first studies were followed by a huge interest of the organic chemistry community with many reports on the development of catalysts based on late-transition metals and, more recently, on first row transition metals [39-47].

Since then, bifunctional catalysts for ATH and AH have aroused a long-term interest for the development of innovative catalysts due to a lack of general solutions for catalytic asymmetric

hydrogenations[48]. The resulting new generations of catalysts, based on both hydrogen bonding, CH-π stacking and ion-pair interactions, have exhibited new functionalities. They have not only allowed bifunctional hydrogen transfer as in the Noyori's early examples[49], but also activation of organic substrates through secondary interactions (cooperative catalysis)[50] or heterolytic activation of dihydrogen itself. At last, several recent theoretical studies[51-53] have emphasized the significant contributions of weak non-covalent attractive interactions between the substrate and the chiral ligand to enantioselection in hydrogenation reactions.

Following the impressive performances of homogeneous ruthenium-based bifunctional catalysts in ATH, Noyori-Ikariya catalysts have gradually been supported on various materials such as silicas, polymers, ionic liquids or micelles for economic, environmental and societal reasons. These heterogenised catalysts have allowed the asymmetric transfer hydrogenation of ketones and imines with high activities and enantioselectivities [54-57]. In addition, they have also been combined with other supported organometallic or organic catalysts to perform effectively tandem reactions combining ATH with various reactions including cross-couplings, aza-Michael reaction, alkyne hydration, lactonisation, oxisulfonylation or oxidation. This article reviews over the past 7 years the development of supported Noyori-Ikariya catalysts based on ruthenium, rhodium and iridium for ATH of various CO and CN unsaturated bonds and related tandem reactions through the use of an additional heterogeneous organometallic or organic catalyst. It highlights and discusses the synthesis, reactivity and performances of these new bifunctional catalysts, as well as their recycling.

2. Catalysts supported on materials and polymers

2.1. Ruthenium based catalysts

2.1.1. ATH

In 2015, Rahman and co-corkers reported a chiral N-sulfonyldiamine ligand supported on mesoporous MCM-41 silica which was combined with $[RuCl_2(p\text{-cymene})]_2$ to catalyse the ATH of several aromatic ketones in water and afford the corresponding alcohols in good yields and enantioselectivities (Scheme 1) [58]. After the reactions, the catalyst was recovered through simple filtration, then subsequently washed with water and ethylacetate, and reused up to four times. Though metal leaching was not examined, no significant loss of activity and enantioselectivity was observed.

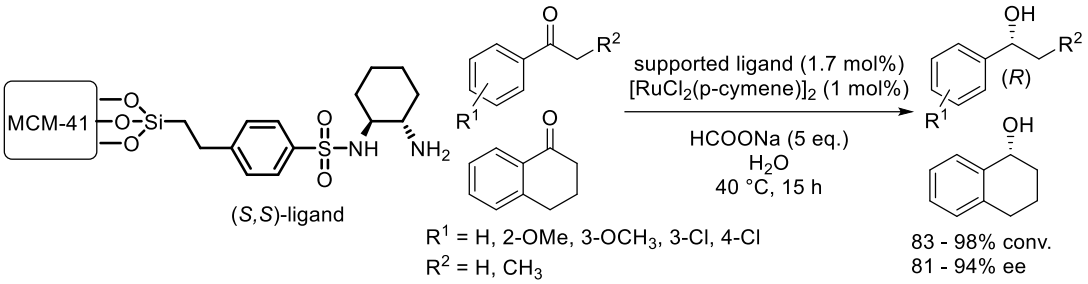

Scheme 1. ATH of ketones in water with mesoporous MCM-41-supported ruthenium catalyst. Reproduced/Adapted from Ref. [58] with permission from Wiley-VCH.

In 2016, Liu and co-workers developed an amphiphilic mesostructured silica functionalised by chiral ruthenium ArDPEN through a self-templating assembled strategy implying the use of amphiphilic poly(ethylene glycol) monomethyl ether-modified hyperbranched polyethoxysiloxane as a silica precursor (Scheme 2) [59]. The resulting mesostructured amphiphilic ruthenium heterogeneous catalyst was highly dispersed in water and effectively catalysed the ATH of acyclic α-trifluoromethylimines providing the chiral α-trifluoromethylamines in good to high yields and high enantioselectivities. The recovery of the catalyst through centrifugation allowed its reuse for seven consecutive runs without any significant change of activity or selectivity.

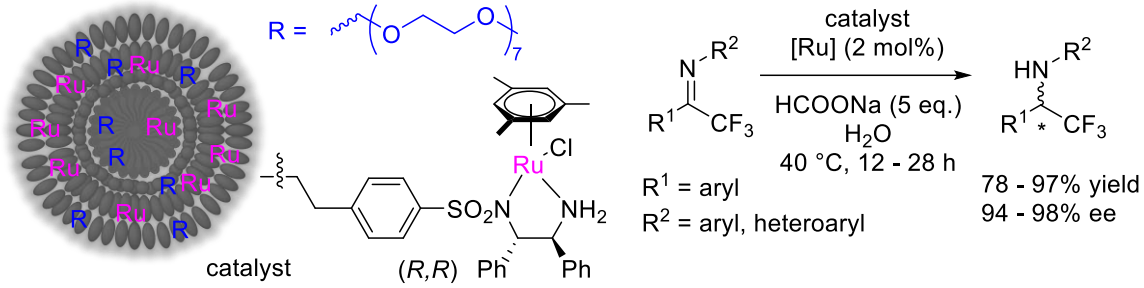

Scheme 2. ATH of imines in water with ruthenium catalysts supported on a functionalised mesostructured silica. Reproduced/Adapted from Ref. [59] with permission from the American Chemical Society.

The same year, Hou and co-workers prepared a new type of ruthenium catalyst for ATH supported on a pH-responsive soluble polymer issued from the copolymerisation of dimethyl

aminopropyl acrylamide and N-p-styrenesulfonyl-1,2-diphenylethylenediamine (Scheme 3) [60]. While the ArDPEN moiety coordinated the ruthenium, the tertiary amine played a cooperative role in pH-induced phase separation and accelerated the ATH of ketones in water. Indeed, such catalyst provided the corresponding alcohols in high yields and enantioselectivities and was effectively recycled for eight runs thanks to its precipitation at pH 8.5. A minor ruthenium leaching of 0.4 ppm was observed according ICP-AES analyses.

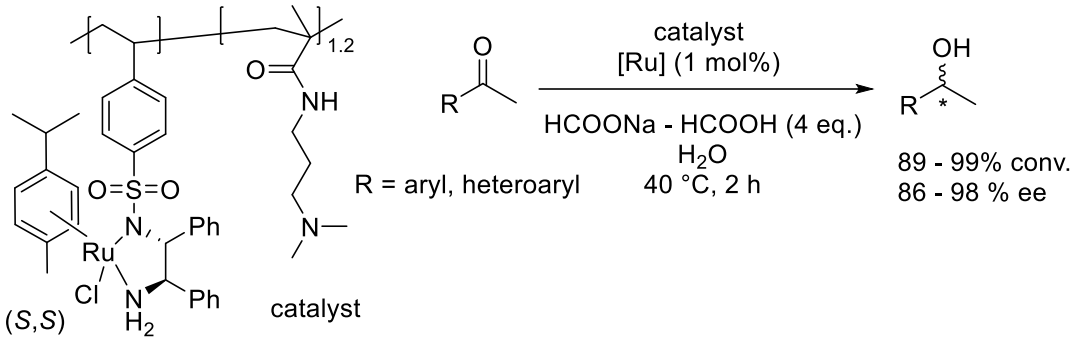

Scheme 3. ATH of ketones using a ruthenium catalyst supported on a pH-responsive soluble polymer. Reproduced/Adapted from Ref. [60] with permission from Wiley-VCH.

Also in 2016, Reiser, Hanson, Pericàs and co-workers immobilised a chiral ArDPEN ruthenium species on carbon-coated magnetic cobalt nanoparticles and applied the resulting material to the ATH of arylketones (Scheme 4) [61]. The nature of the polymer matrix serving as linker between the magnetic support and the catalytic species proved to have a strong influence on the catalytic activity, the best results being obtained when a vinyl group of the organic ArDPEN ligand was copolymerised with divinylbenzene and a vinylbenzene functionalised support. The catalysed ATH provided the corresponding chiral alcohols in good to high yields and high enantioselectivities for up to ten consecutive runs. Thanks to its magnetic properties, the catalyst was effectively recovered and reused, but a gradual decrease in yields was observed from the sixth run due to a ruthenium leaching of 6% over ten runs which however remained below the 10 ppm ruthenium contamination threshold in pharmacy.

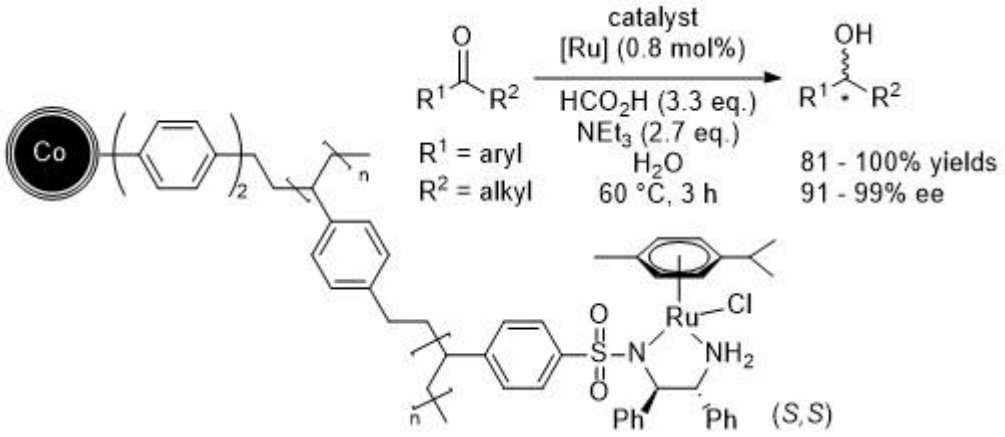

Scheme 4. ATH of ketones in water with magnetic ruthenium catalysts. Reproduced/Adapted from Ref. [61] with permission from the American Chemical Society.

In 2020, Canivet and co-workers reported the functionalisation of MIL-101 metal–organic framework with a chiral peptide to host a Noyori-type chiral ruthenium catalyst which performed better than its homogeneous counterpart (Scheme 5) [62]. At 20°C, the ATH of acetophenone led to the corresponding (*S*)-phenylethanol in low yield and enantioselectivity but a reaction performed at 60 °C resulted in a 90% yield though its enantioselectivity remained low. A computational study pointed out the critical role of both the peptide ligand and the support in enhancing the enantioselection by favorising face-specific host–guest interactions with the acetophenone substrate. The spent catalyst was not analysed, nor reused.

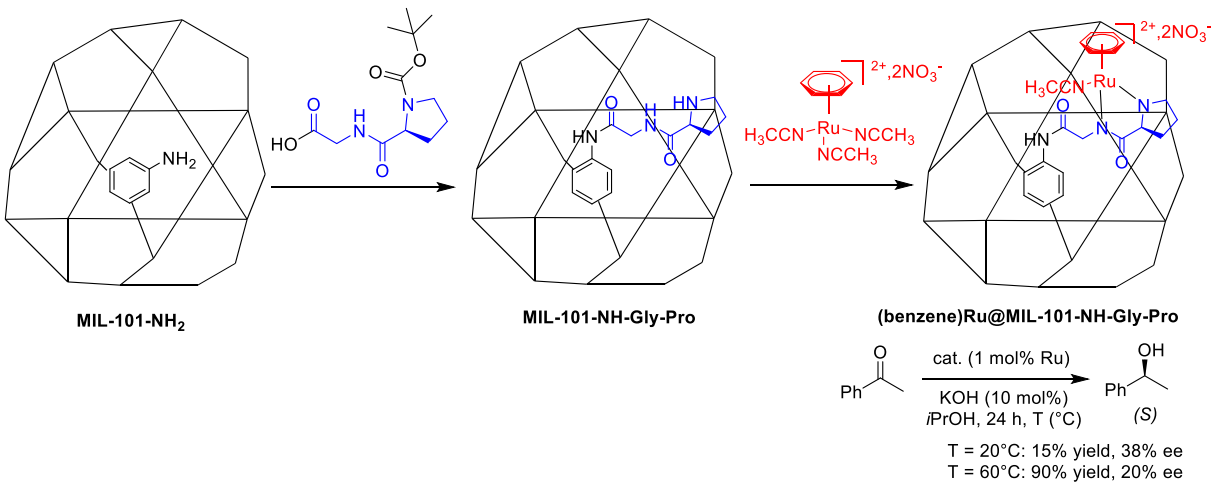

Scheme 5. ATH of ketones with a ruthenium catalyst hosted in a metal-organic framework. Reproduced/Adapted from Ref. [62] with permission from The Royal Society of Chemistry.

In 2021, Doherty, Knight and co-workers anchored a Noyori-Ikariya TsDPEN-(arene)Ru(II) catalyst on amorphous silica and DAVISIL (Scheme 6) [63]. They proceeded by using a tether connecting the η^6-coordinated arene ligand to the support via a straightforward synthesis. Applications of the resulting materials to the ATH of various ketones under mild reaction conditions revealed the catalyst supported on DAVISIL was more active than the one on amorphous silica affording the corresponding alcohols in good to high conversions and high enantioselectivities with turnover frequencies (TOF) between 71 and 118 h^{-1}. In spite of an initial TOF of 1085 h^{-1}, the catalyst activity decreased within the next hours of use. This trend was confirmed by the recycling study over which the catalyst was recovered for 5 cycles by using centrifugation with ethylacetate. Indeed, although high enantioselectivities were maintained throughout the cycles, the conversions decreased gradually along the runs to 60% due to the gradual leaching of the ruthenium.

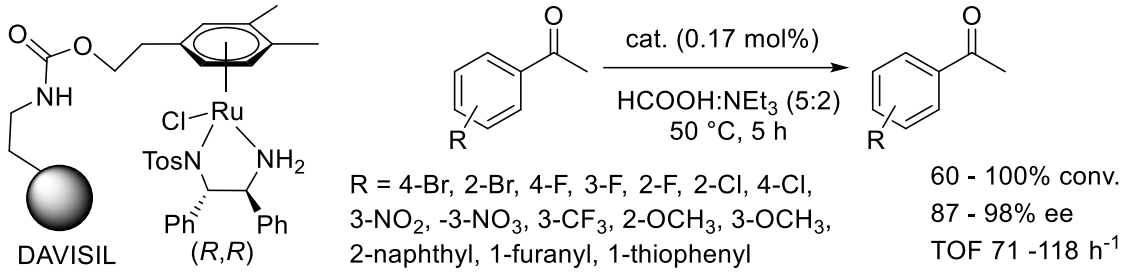

Scheme 6. ATH of ketones with a ruthenium catalyst supported on DAVISIL. Reproduced/Adapted from Ref. [63] with permission from Wiley-VCH.

In 2022, Jia and co-workers prepared a thermoresponsive chiral block copolymer on the surface of β-cyclodextrin (CD) by copper catalysed ATRP controlled polymerisation (Scheme 7) [64]. The molecular weight and distribution of the resulting star–shaped polymers were controlled through self-catalysis of chiral monomers and polymers. Furthermore, a chiral amplification effect was noticed by circular dichroism spectroscopy upon coordination of the prepared star–shapped polymer ligands to Cu(II) cations. The subsequent coordination of the long chain copolymer ligand to ruthenium resulted in single-chain nanostructures which could undergo in water a self-folding process and led to small nanoparticles of 4-10 nm as shown by dynamic light scattering (DLS) and TEM analyses. Interestingly, a synergistic effect between ruthenium and copper enhanced the activity and enantioselectivity of the nanocatalyst in the

ATH of alkyl and arylketones in water by comparison to the related ruthenium catalyst under homogeneous conditions. Finally, the catalyst could be precipitated by increasing the temperature and reused up to six times with similar catalytic performances and without any significant leaching according ICP analysis.

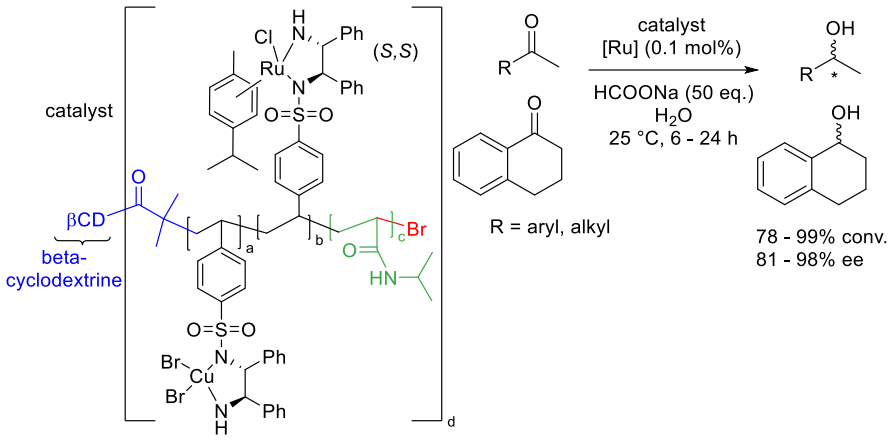

Scheme 7. ATH of ketones in water with bimetallic copper and ruthenium catalyst supported on a thermoresponsive chiral block copolymer linked to a β-cyclodextrin. Reproduced/Adapted from Ref. [64] with permission from Elsevier.

2.1.2. Tandem reactions

In 2016, Liu and co-workers applied a yolk-shell mesoporous silica for the immobilisation of two catalysts: a chiral ArDPEN-ruthenium in the yolk part and a palladium diphosphine dispersed in the silica shell that was coated by an hydrophobic layer formed by silicon ethylene-linkers (Scheme 8) [65]. The resulting dual catalyst was well-dispersed in MeOH/H_2O (3:1) and applied to the one-pot tandem reaction implying first a palladium catalysed Sonogashira cross-coupling of iodo-arylketones with aryl or alkyl alkynes followed by a ruthenium catalysed ATH of the formed alkynyl-arylketones. The resulting conjugated alkynols were obtained in high yields and enantioselectivities. This supported dual catalyst performed better than a mixture of the homogeneous counterparts and was reused in eight consecutive runs without significant loss of activity or selectivity, and with rather low palladium and ruthenium leachings of respectively 7.5% and 4.8% after the eighth recycling.

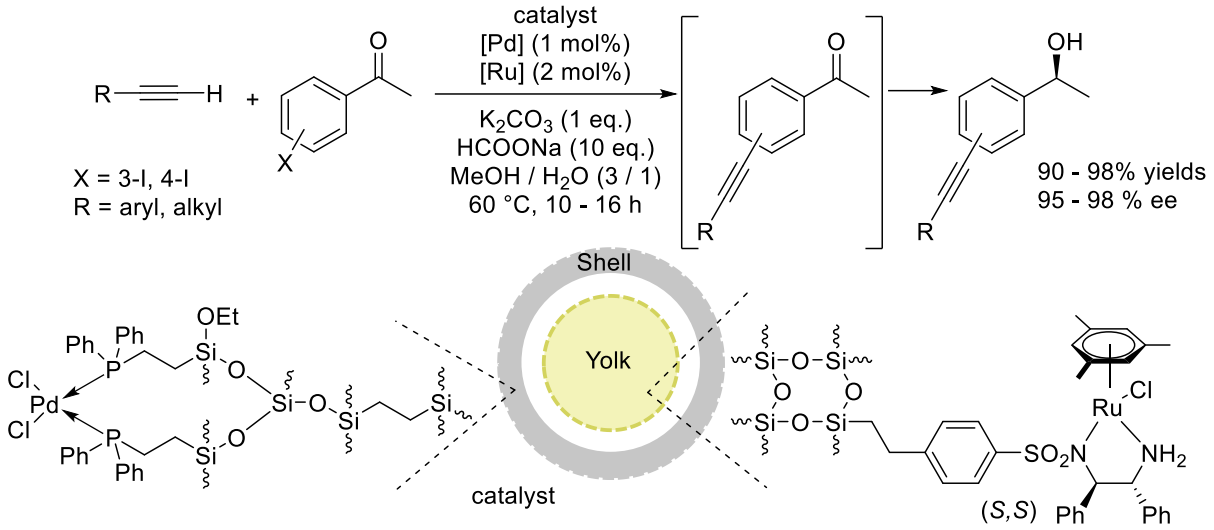

Scheme 8. Tandem Sonogashira cross-coupling and ATH with palladium and ruthenium catalysts supported on a yolk-shell mesoporous silica. Reproduced/Adapted from Ref. [65] with permission from The Royal Society of Chemistry.

A year after, Liu and co-workers prepared a mesoporous solid comprising a ruthenium ArDPEN species and a cetyl−trimethylammonium chloride surfactant (Scheme 9) [66]. According to microscopy analyses, the resulting material displayed a uniform distribution of the ruthenium species in the mesopores. The dual heterogeneous catalyst achieved in a one-pot procedure the nucleophilic substitution of α−bromoketones and sodium sulfonates followed by the ATH of the 1-substituted-2-(phenylsulfonyl)ethanone to form the desired chiral β−hydroxy sulfones in good to high yields and enantioselectivities. The heterogeneous catalyst was recovered through centrifugation and reused effectively until the sixth run, a significant decrease of yield being observed for the seventh run due to a large ruthenium leaching of 12%.

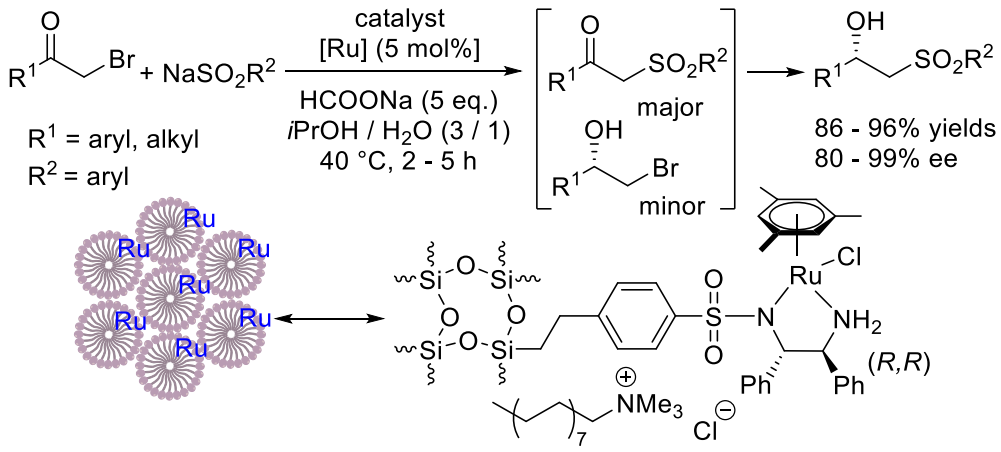

Scheme 9. Tandem nucleophilic substitution and ATH with a cetyl−trimethylammonium chloride surfactant combined to a ruthenium catalyst on a mesoporous solid. Reproduced/Adapted from Ref. [66] with permission from The Royal Society of Chemistry.

The same year, Liu and co-workers developed a heterogeneous bifunctional catalyst supported on hydrophobic ethylene coated periodic mesoporous silica by combining palladium nanoparticles coordinated to propane-1-thiol ligands with a ruthenium ArDPEN species (Scheme 10) [67]. Structural analyses confirmed that the resulting catalyst had an ordered mesostructure with dispersed active species. The one-pot tandem ruthenium catalysed ATH of iodo-arylketones and palladium catalysed Sonogashira cross-coupling of the resulting iodo-arylalcohols with arylalkynes was confirmed by kinetic studies and afforded conjugated alkynols in high yields and enantioselectivities. The catalyst was reused for seven consecutive runs without significant loss in yield or enantioselectivity, but a further run resulted in a lower yield due to a strong palladium leaching of 12%.

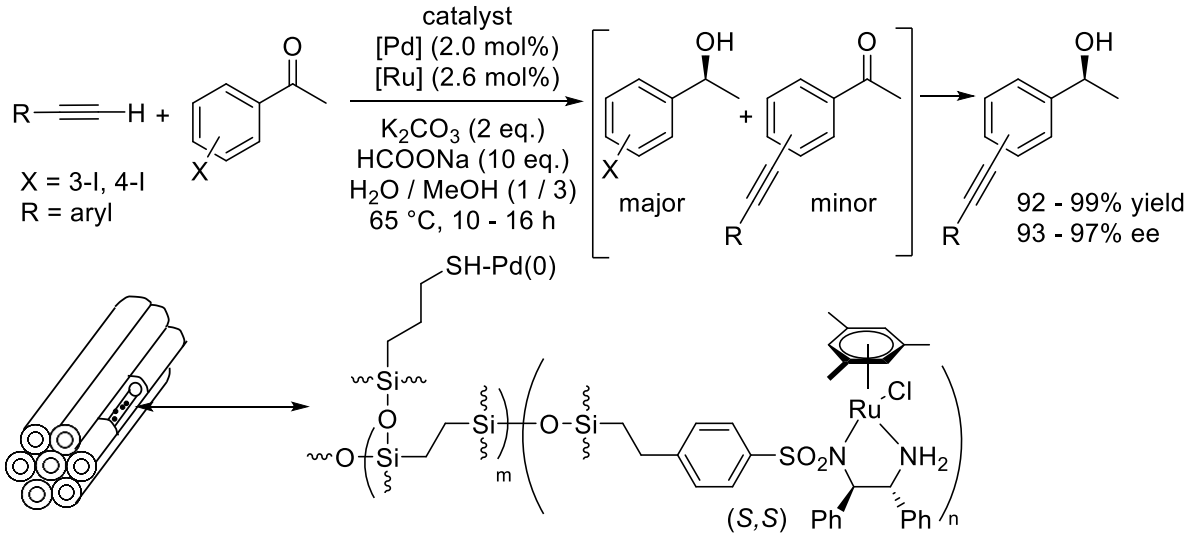

Scheme 10. Tandem Sonogashira cross-coupling and ATH with palladium and ruthenium catalysts supported on bifunctionalised periodic mesoporous organosilica. Reproduced/Adapted from Ref. [67] with permission from The Royal Society of Chemistry.

Still in 2017, Liu and co-workers reported another strategy to immobilise two different active centers within the nanopores of the mesoporous silica FDU-12 (Scheme 11) [68]. While

a cationic gold NHC species was supported through hydrogen-bonding between its BF_4 counteranion and the silanols of the inner surface, a ruthenium ArDPEN species was covalently bonded within the nanochannels. Microscopy analyses highlighted that gold and ruthenium species were uniformly distributed in the mesoporous silica. The resulting multifunctional and cooperative catalyst was applied to the one-pot hydration–ATH of haloalkynes and afforded halohydrins in high yields and enantioselectivities. The recycling of the catalyst was possible through centrifugation and no significant loss of activity or selectivity was noticed along seven consecutive runs but a further run led to a lower yield due to significant leachings of gold (12%) and ruthenium (7%).

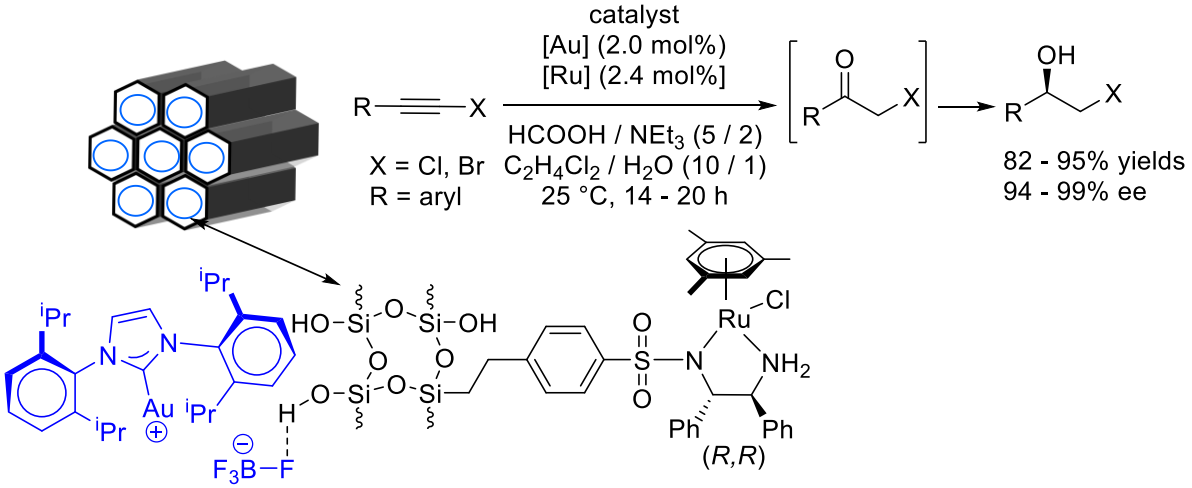

Scheme 11. Tandem alkyne hydration and ATH with a dual gold–ruthenium catalysts supported on large periodic mesoporous organosilica. Reproduced/Adapted from Ref. [68] with permission from The Royal Society of Chemistry.

In 2018, Liu and co-workers immobilised DABCO and ArDPEN-ruthenium catalysts through hydrogen bondings in the nanopores of a trimethysilylated silica FDU−12 composite (Scheme 12) [69]. The aza-Michael addition of aniline derivatives to aryl-substituted enones was catalysed by the Lewis base and formed the corresponding amino-ketones that were subsequently reduced by ruthenium catalysed ATH. Thanks to this synergistic tandem reaction, chiral γ-secondary amino alcohols were obtained in good to high yields and high enantioselectivities. The catalyst was recovered through centrifugation and reused for five

consecutive runs without significant loss of activity or selectivity. However, a further sixth run led to a lower yield due to a significant ruthenium leaching of 12%.

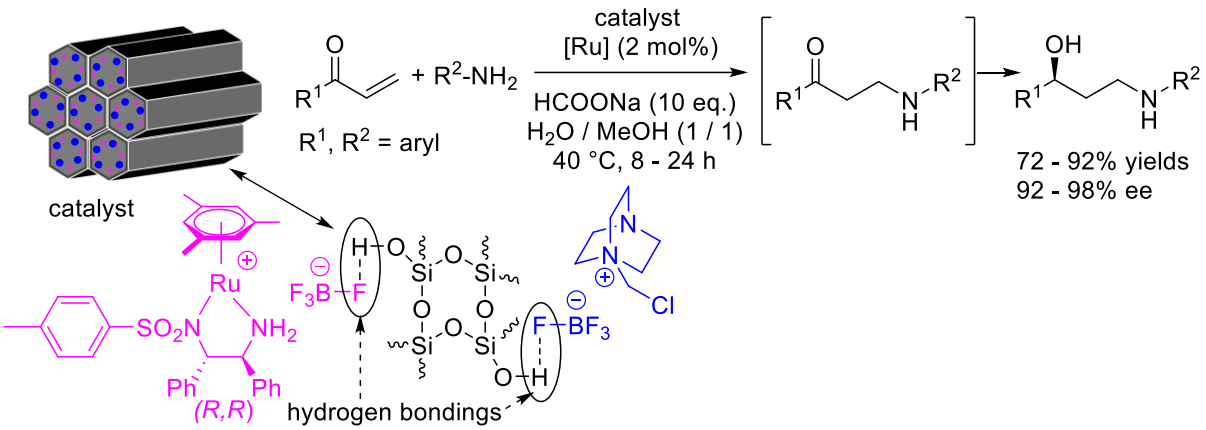

Scheme 12. Tandem aza-Michael reaction and ATH with a dual DABCO–ArDPEN-ruthenium catalyst hydrogen bonded on large periodic mesoporous organosilica. Reproduced/Adapted from Ref. [69] with permission from Frontiers Media S.A.

The same year, Liu and co-workers developed a yolk-shell-mesostructured silica-support to promote a site-isolating strategy for the immobilisation of two different metal-based catalysts, palladium/carbon nanoparticles dispersed in the yolk part and chiral ArDPEN-ruthenium in the silica shell which was coated by a hydrophobic silicon ethylene layer (Scheme 13) [70]. The resulting dual catalyst was applied to the concomitant reduction of the alkyne and ketone functions of 4-(arylethynyl)phenylethanones to lead to the corresponding chiral arylethyl-substituted aromatic alcohols in high yields and enantioselectivities. The catalyst was recovered and reused for six consecutive runs without significant loss of activity or selectivity, but a seventh run led to a lower yield due to a significant palladium leaching of 12%.

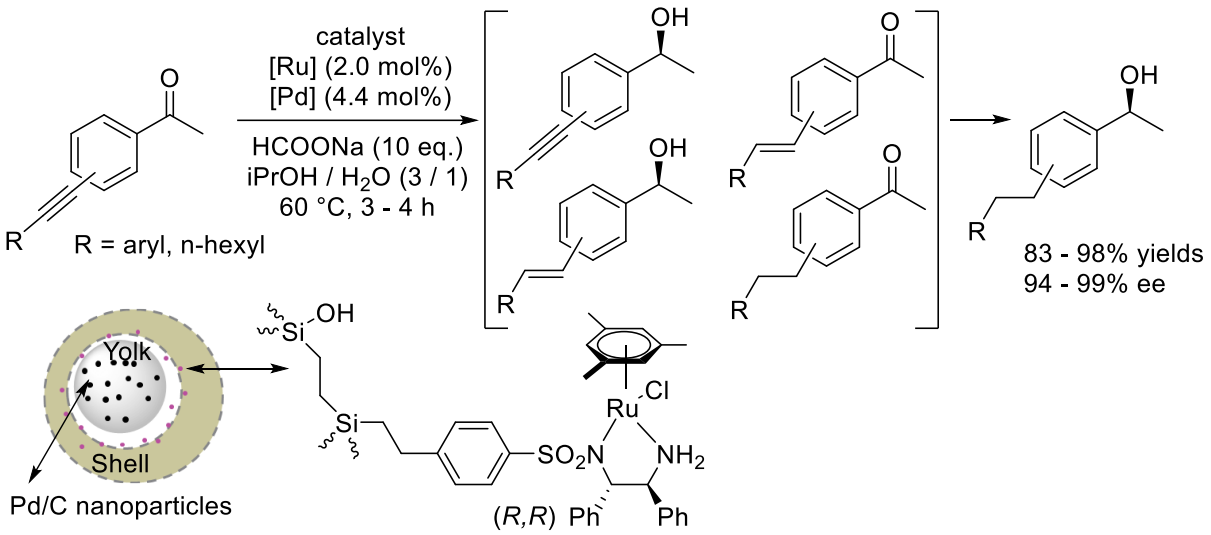

Scheme 13. Tandem hydrogenation of alkyne and ATH of ketone with a dual palladium–ruthenium catalyst supported on a yolk-shell-mesostructured silica. Reproduced/Adapted from Ref. [70] with permission from The Royal Society of Chemistry.

At about the same period, Liu and co-workers applied a similar yolk-shell-mesostructured silica-support for the separated immobilisation of two catalysts, a chiral ruthenium ArDPEN and a basic DABCO, respectively immobilised in the silicate yolk and shell in a uniform way (Scheme 14) [71]. While DABCO catalysed aza-Michael reactions of enones with primary amines, the ruthenium catalyst allowed the ATH of the resulting amino-ketones to afford aryl–substituted γ–secondary amino alcohols in good to high yields and high enantioselectivities. Furthermore, the catalyst was applied in a continuous flow process, but a decreased reactivity was observed after 5.5 h of run due to a significant ruthenium leaching of 10% according ICP-AES analysis.

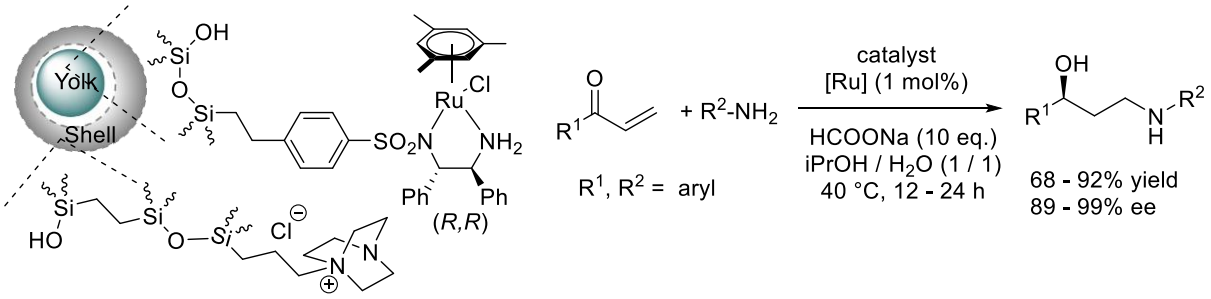

Scheme 14. Tandem aza-Michael – ATH under flow with DABCO and ruthenium catalysts supported on a yolk-shell-mesostructured silica. Reproduced/Adapted from Ref. [71] with permission from Wiley-VCH.

In parallel, Liu and co-workers applied again hollow-shell mesoporous silica nanospheres to immobilise two different active catalysts (Scheme 15) [72]. Whereas an ionic palladium NHC species was supported through hydrogen-bonding between its BF_4 anion and the silanols of the inner surface, a ruthenium ArDPEN species was covalently bonded within the nanochannels. Microscopy analyses highlighted the palladium and ruthenium species were uniformly distributed within the dispersed silica nanospheres. The resulting hetero-bifunctional catalyst was applied to a tandem Suzuki cross-coupling – ATH reaction to form chiral biaryl alcohols in good to high yields and high enantioselectivities. It was worth to note the negative interference of the two catalytic species observed under homogeneous conditions was overcome through the hydrophobic effect of the silicon ethylene coating which was used here to protect the outer silanols with trimethysilyl (–$SiMe_3$) groups. The catalyst recycling through centrifugation allowed to perform six consecutive runs without any significant change of activity and selectivity. Finally, the use of the large pyren-1-ylboronic acid led to a much lower yield (18%) due to a size selectivity implied by the steric restrictions of the nanopores.

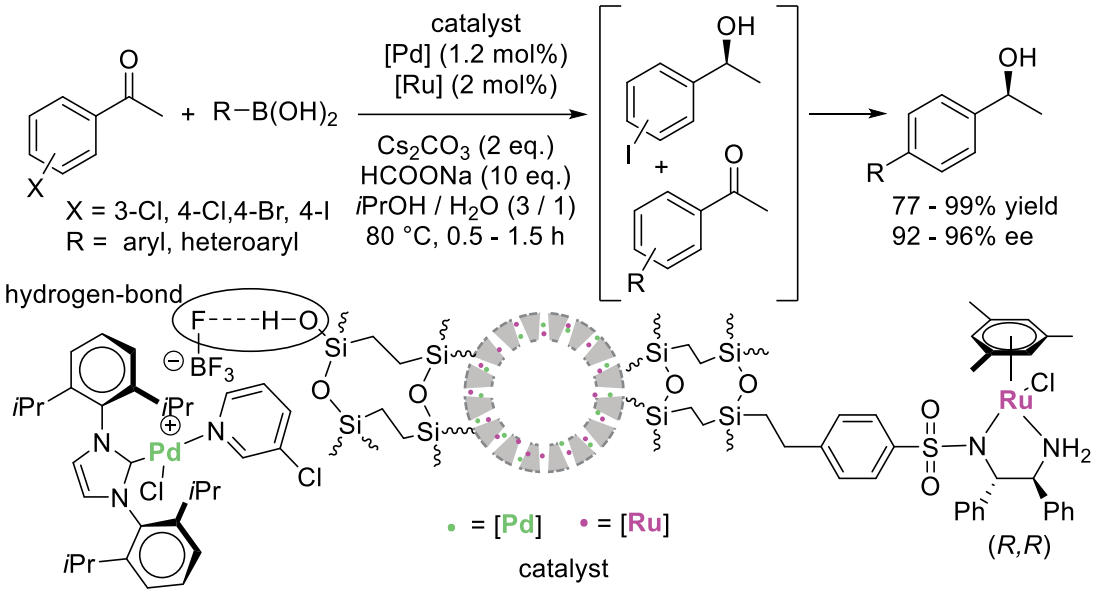

Scheme 15. Tandem Suzuki cross-coupling – ATH with palladium and ruthenium catalysts supported on hollow-shell mesoporous silica nanospheres. Reproduced/Adapted from Ref. [72] with permission from The Royal Society of Chemistry.

Through another approach, Liu and co-workers reported another bifunctional catalyst for a tandem Suzuki cross-coupling–ATH based on monodisperse mesoporous silica

nanoparticles (Scheme 16) [73]. Following a three-component self-assembly procedure, a palladium phosphine and a chiral ruthenium ArDPEN species were incorporated uniformly in a hyperbranched polyethoxysiloxane support functionalised by amphiphilic poly(ethylene glycol)monomethyl ether. The resulting material exhibited two well-defined active centres and achieved an enantioselective one-pot tandem reaction by combining palladium catalysed Suzuki cross-coupling and ruthenium catalysed ATH. The resulting chiral biaryl alcohols were isolated in high yields and enantioselectivities and the catalytic material was recovered and reused in eight consecutive runs without significant loss of activity or selectivity. However, a further run led to a lower yield due to a significant ruthenium leaching of 13%.

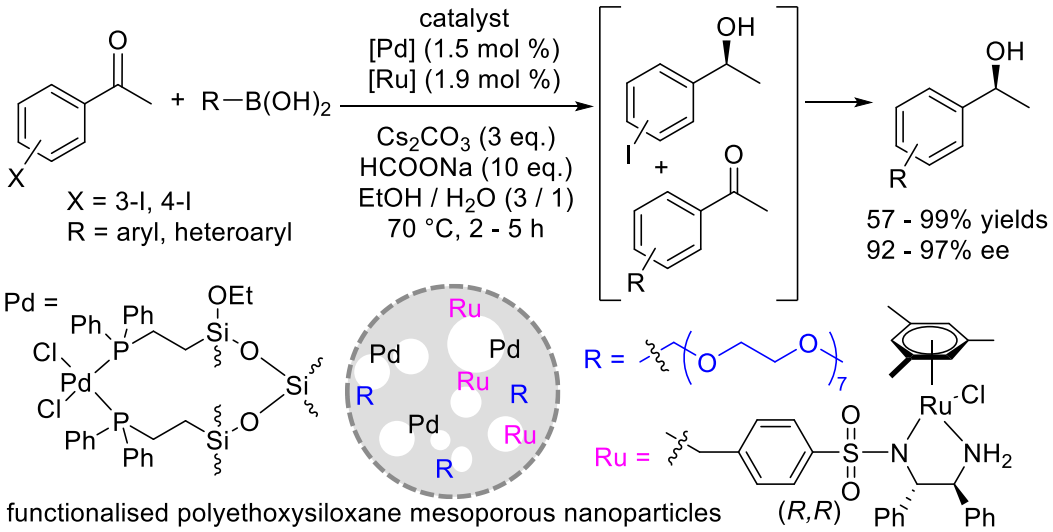

Scheme 16. Tandem Suzuki cross-coupling–ATH with palladium and ruthenium catalysts supported on monodisperse mesoporous silica nanoparticles. Reproduced/Adapted from Ref. [73] with permission from Wiley-VCH.

In 2019, Liu and co-workers developed a bifunctional catalyst with a magnetic yolk–shell mesoporous structure containing a well-dispersed Pd/C species in the inner yolk and a chiral ruthenium ArDPEN species in the nanochannels of the outer silica shell (Scheme 17) [74]. Two tandem catalytic processes were investigated: a first that combined a Suzuki cross-coupling of iodoacetophenones and arylboronic acids with an ATH reduction process and, a second that started from styryl-substituted aromatic ketones and allowed the hydrogenation of alkenes and the ATH of ketones. In both cases, the corresponding alcohols were obtained in high yields and enantioselectivities. Thanks to its magnetic properties, the catalyst was easily

recovered using an external magnet and reused in 10 consecutive runs. If activities and selectivities were rather stable for nine runs, a significant drop of the yield was observed in the tenth run due to a significant ruthenium leaching of 11.3% according to ICP-AES analyses.

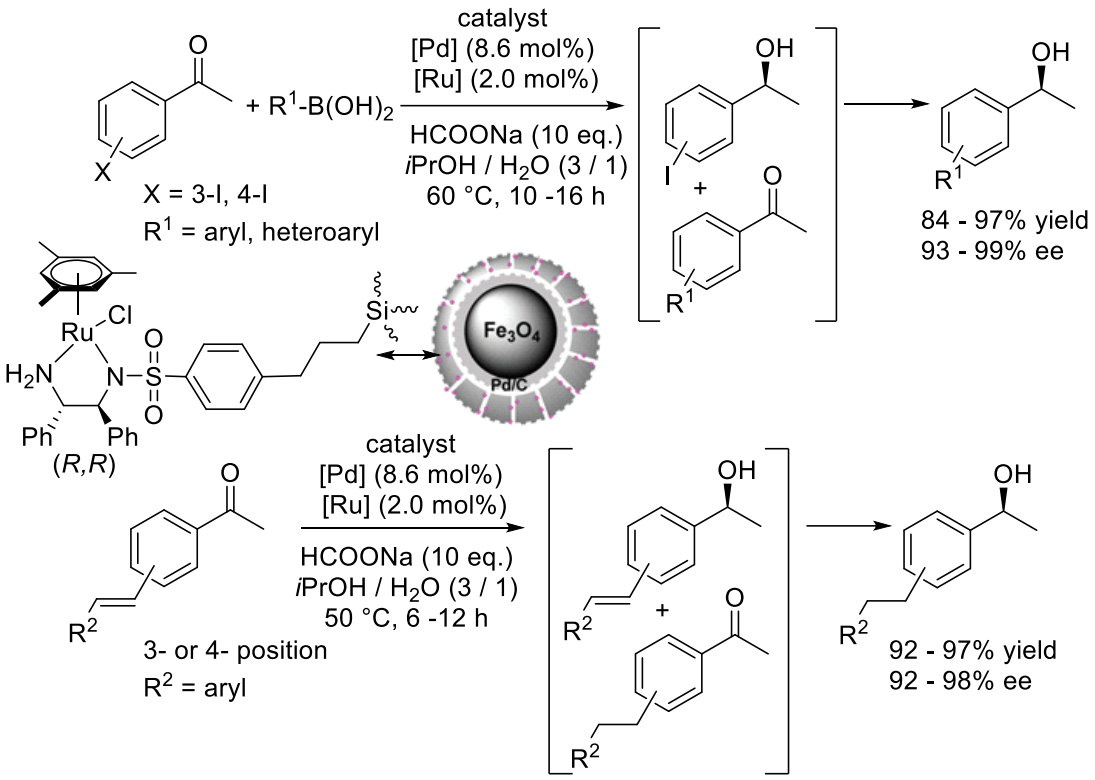

Scheme 17. Tandem Suzuki cross-coupling–ATH or transfer hydrogenation–ATH with dual palladium–ruthenium catalysts supported on magnetically retrievable mesoporous silica. Reproduced/Adapted from Ref. [74] with permission from The Royal Society of Chemistry.

The same year, Liu and co-workers reported two dual switchable catalytic systems for two different tandem reactions (Scheme 18) [75]. A first example implied the immobilisation of a bis amido-bisphosphino-palladium species on the outer surface of silica nanoparticles, and of a ruthenium ArDPEN species in the nanochannels of thermoresponsive polymer-coated hollow-shell mesoporous silica nanoparticles. Interestingly, depending on the temperature, the polymer coating layer localised on the external surface of the silica shell could open or close the entrances of the nanochannels and, respectively switch on or off, the ruthenium catalyst, in order to perform Suzuki cross-couplings followed by ATH in a single-pot. Therefore, starting from iodo-acetophenones at 60°C, the palladium species catalysed the cross-coupling reaction

to lead to biphenyl-ethanone derivatives, which were subsequently reduced in situ at 15°C by the chiral ruthenium ArDPEN species to afford the corresponding secondary alcohols in high yields and enantioselectivities. The second example relied on the immobilisation of primary amide functions on the outer surface of silica nanoparticles, and of ruthenium ArDPEN species in the nanochannels of thermoresponsive polymer-coated hollow-shell mesoporous silica nanoparticles. By comparison to the first example, a different polymer coating layer on the external surface of the silica shell could adopt an unfolded conformation at 35°C and therefore switch on the ruthenium catalyst. Hence, starting from arylpropenones and arylamines at 15°C, the basic primary amide catalysed the aza-Michael reaction to form amino-ketones which were subsequently reduced in the same vessel at 35°C by the chiral ruthenium ArDPEN species to afford the corresponding secondary alcohols in high yields and enantioselectivities. Both dual catalytic systems were used for six consecutive runs without significant decrease of activities and selectivities.

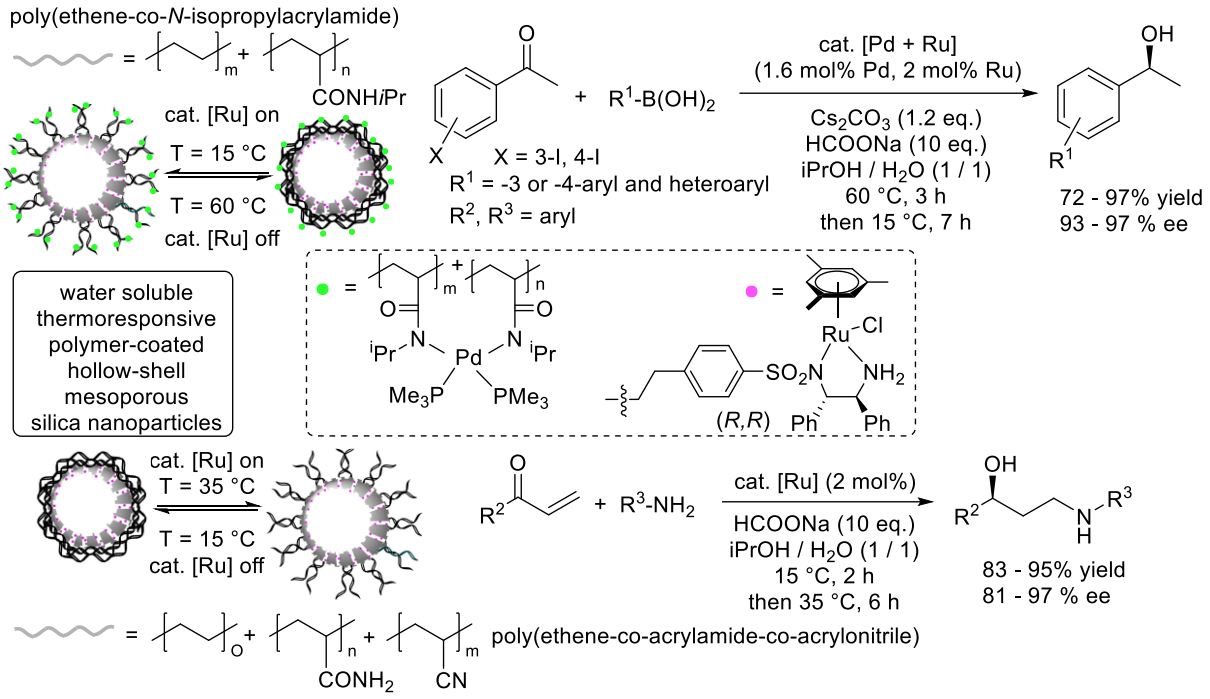

Scheme 18. Tandem Suzuki cross-coupling–ATH or aza-Michael–ATH with switchable catalysts comprising ruthenium associated with palladium or an organocatalyst. Reproduced/Adapted from Ref. [75] with permission from the American Chemical Society.

In parallel, Liu and co-workers followed another approach to develop a one–pot enantioselective aza–Michael addition–ATH tandem reaction using an heterobifunctional catalyst integrated on a double–type support (Scheme 19) [76]. The aza–Michael addition between aryl–substituted enones and aniline derivatives was catalysed by tertiary amine functions tethered on soluble polymer chains, which were set on the outer sphere of mesoporous silicate nanoparticles. The resulting amino-ketone products were subsequently reduced by ATH catalysed by a ruthenium ArDPEN catalyst grafted in the inner channels of the mesoporous silicate nanoparticles. The resulting aryl–substituted γ–secondary amino alcohols were obtained in good to high yields and enantioselectivities. Both active species of this heterobifunctional catalyst were well isolated and this allowed tandem reactions to proceed under mild conditions using isopropanol and water as solvents. The catalyst was recovered through centrifugation and reused for seven consecutive runs. Interestingly, yields and enantioselectivities decreased only at the seventh run due to a ruthenium leaching of about 13% according analyses by ICP-AES.

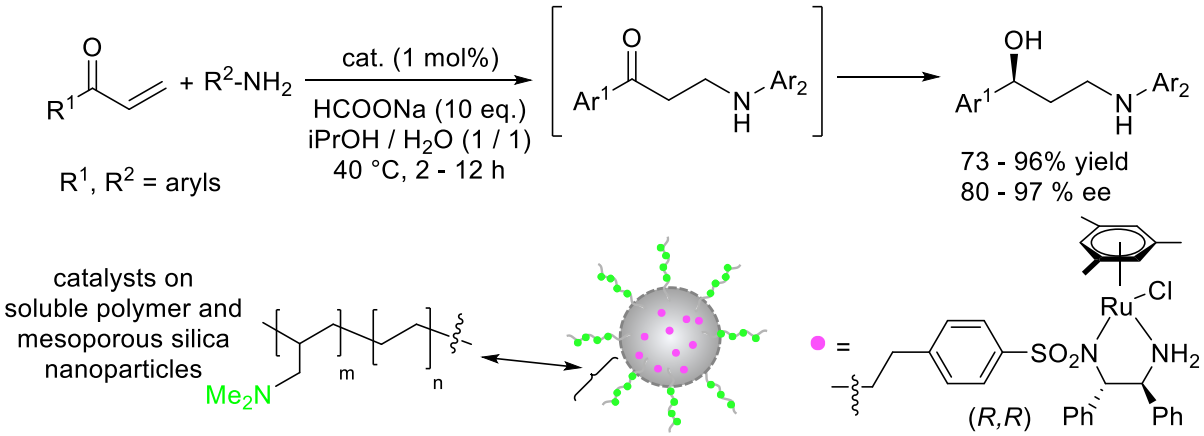

Scheme 19. Tandem aza-Michael–ATH with an organocatalyst and a ruthenium catalyst on a soluble polymer combined with a mesoporous silica. Reproduced/Adapted from Ref. [76] with permission from Elsevier.

In 2021, Liu and wo-workers reported a dual aerobic oxysulfonylation–ATH catalytic process (Scheme 20) [77]. The first reaction between aryl-substituted alkynes and sodium sulfinates was catalysed by $FeCl_3$ species immobilised in the inner core of a yolk-shell-structured magnetic mesoporous silica. The resulting β-keto sulfones intermediates were subsequently hydrogenated in situ by the ArDPEN–ruthenium catalyst supported into the

nanochannels of the outer mesoporous silica shell to afford β-hydroxysulfones in good to high yields and high enantioselectivities. Noteworthy, the catalysts immobilisation through a compartmentalisation strategy allowed the sequential catalytic process by overcoming the negative cross-interactions between iron and ruthenium species. The dual catalyst was easily recovered through the use of an outer magnet and effectively recycled for 5 cycles. However, after the sixth run, the product yield decreased and a significant ruthenium loss of 7.3% was detected according to ICP-AES analysis.

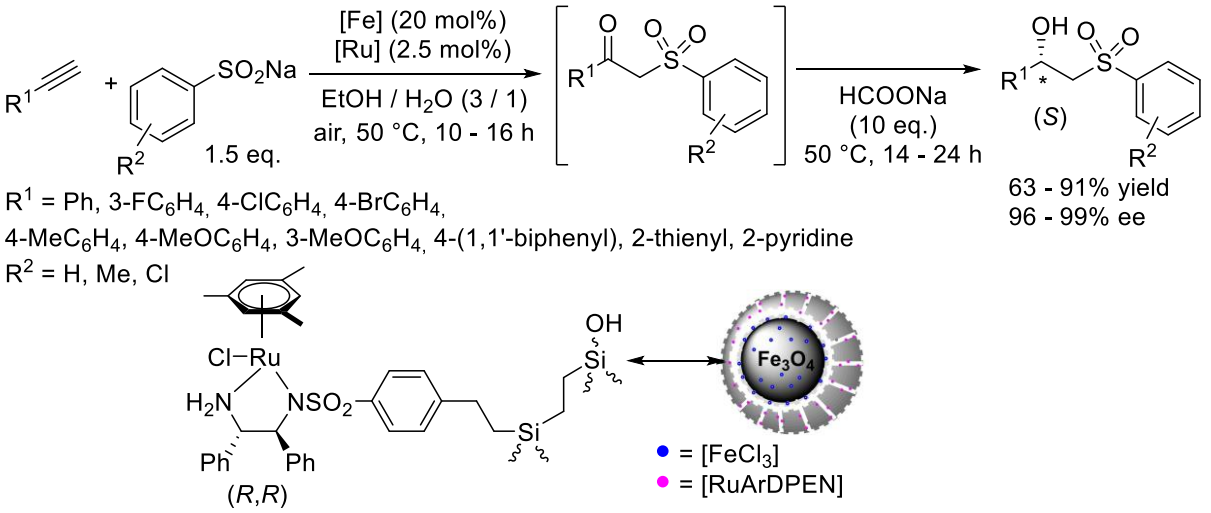

Scheme 20. Tandem aerobic oxysulfonylation–ATH with a dual iron–ruthenium catalyst supported on a yolk-shell-structured magnetic mesoporous silica. Reproduced/Adapted from Ref. [77] with permission from Wiley-VCH.

The same year, Liu, Tan and co-workers published a sequential hydration–ATH catalytic process for the one-pot synthesis of valuable chiral alcohols from alkynes (Scheme 21) [78]. At first, they applied homogeneous cobaloxime to catalyse the hydration of phenylacetylene derivatives to aromatic ketones. The latter were subsequently reduced through ATH by using a heterogeneous ArDPEN–ruthenium catalyst supported on dendritic mesoporous organosilica nanoparticles (DMONs) to lead to the corresponding aromatic alcohols in good to high yields and good to high enantioselectivities. The sequential mode was critical in achieving high yields, the cobalt catalyst deactivating the ruthenium counterpart. Though the homogeneous cobaloxime could not be recovered, the reuse of immobilised ruthenium catalyst was studied. After recovery through filtration, the procedure implied the

spent catalyst was Soxhlet extracted with methanol and DCM and then reactivated at 60°C under vacuum. By studying the sequential hydration-ATH of phenylacetylene, authors noticed a stable enantioselectivity but the conversions dropped gradually along the recyclings due to ruthenium leaching as confirmed by ICP-AES analyses of the reaction solutions. By comparison to other ruthenium supported catalysts for ATH, this catalyst immobilised on dendritic mesoporous organosilica nanoparticles (DMONs) had a lower ruthenium content of 0.4 mol%, the loading of similar ruthenium catalysts supported on SBA-15 or FDU-12 being of 1 mol%. However, the fact that catalytic activities and enantioselectivities were very similar, suggested the critical and positive effect of the support, which has a large pore size, highly accessible surface areas and efficient mass transfer, thanks to its central-radical pore structure.

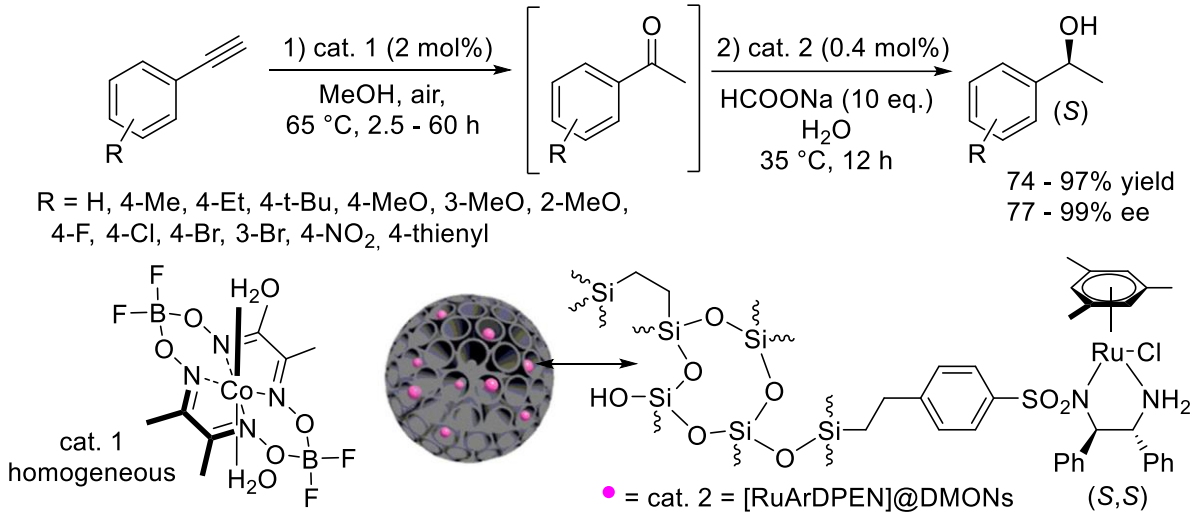

Scheme 21. Tandem hydration–ATH with a homogeneous cobalt catalyst and a ruthenium catalyst supported on dendritic mesoporous organosilica nanoparticles. Reproduced/Adapted from Ref. [78] with permission from Frontiers Media S.A.

In parallel, Liu, Tan and co-workers also developed a dual continuous-flow process, which implied first a palladium-catalysed Suzuki cross-coupling reaction and then a ruthenium-catalysed ATH (Scheme 22) [79]. A palladium–IPrNHC–(3–chloropyridine) species was supported on a periodic mesoporous organosilica and packed in a first column reactor. The second column reactor comprised the ArDPEN-ruthenium catalyst immobilised on another periodic mesoporous organosilica-(PMO). Thus, the two-step organic transformation performed well through cross-coupling of parachloroacetophenone and aryl boronic acids

followed by ATH of the resulting biarylketones and afforded the related biarylols in high yields and enantioselectivities. However, after 10 hours of continuous run, the process activities and selectivities decreased with the appearance of biarylketone intermediate and hydrogenated para–chloroacetophenone. According ICP-AES analyses, the leachings of palladium and ruthenium were minor in product solutions but much higher on both catalyst supports. Nevertheless, this dual continuous-flow process gave higher yields and enantioselectivities than the related homogeneous catalysts and resulted in an attractive up-scaled synthesis of biarylols.

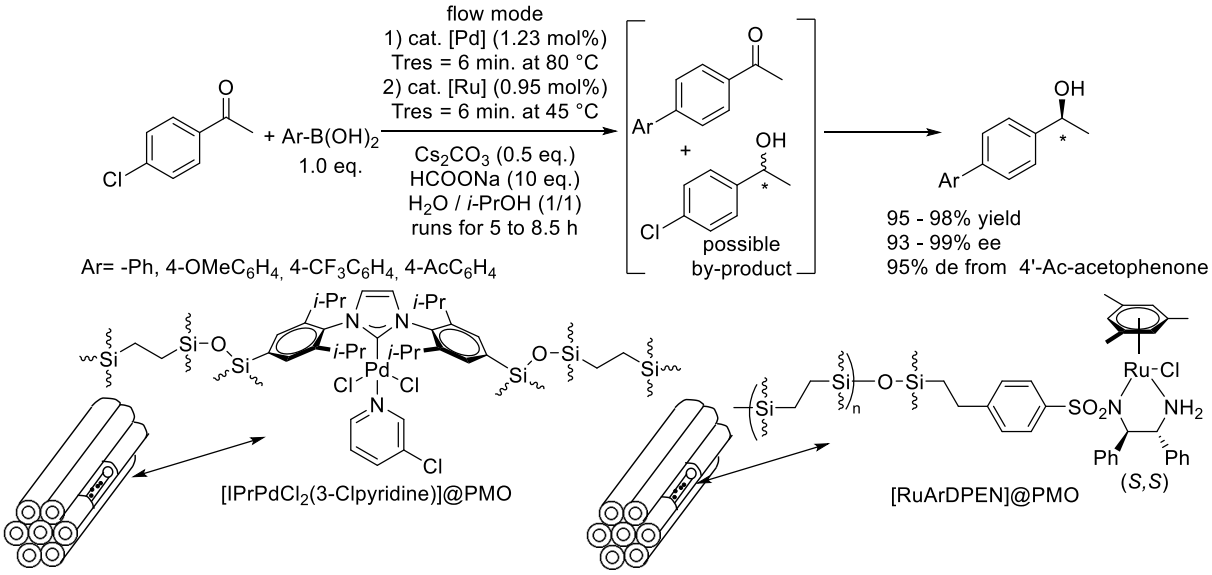

Scheme 22. Tandem Suzuki cross-coupling–ATH under flow with a dual palladium–ruthenium catalyst supported on periodic mesoporous organosilicas. Reproduced/Adapted from Ref. [79] with permission from Wiley-VCH.

2.2. Rhodium based catalysts

2.2.1. ATH

In 2015, Yang and co-workers followed a new strategy to immobilise a rhodium Noyori-Ikariya catalyst by polymerising in situ a styryl-DPEN ligand with divinylbenzene on the silica composite FDU-12 (Scheme 23) [80]. After metallation with $[Cp^*RhCl_2]_2$, analyses by transmission electron microscopy revealed that both the support and the polymer had a uniform and well-defined cubic mesostructure with most of the monomers polymerised inside the material pores. Applications to the ATH of arylketones revealed the composite catalyst had a

much higher activity than the related homogeneous catalyst when the ratio of monomers, i.e. divinylbenzene / (1*R*,2*R*)-N-(4-vinylbenzenesulfonyl)-1,2-diphenylethane-1,2-diamine, was set to 0.17 due to a better polymer dispersion inside the pores. Moreover, the composite had an hydrophilic outer-surface and an hydrophobic inner surface that improved the diffusion of hydrophobic organic reactants in water. Upon recycling this catalyst for 6 cycles, the enantioselectivity remained stable but a gradual decrease of catalytic activity was observed. The reason of the deactivation process was not investigated but longer reaction times allowed the ATH completion.

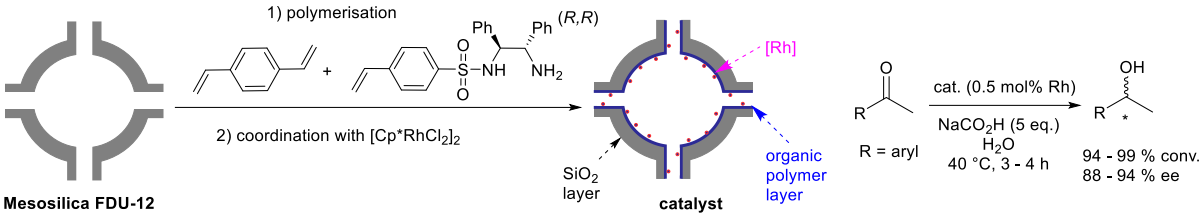

Scheme 23. ATH of ketones in water with DPEN-rhodium catalyst supported on polymer coated silica composite FDU-12. Reproduced/Adapted from Ref. [80] with permission from The Royal Society of Chemistry.

A year after, Liu and co-workers developed a seminal approach by combining on a periodic mesoporous organosilica a Cp*RhArDPEN complex with an imidazolium displaying hydrophobic and phase-transfer properties (Scheme 24) [81]. According to X-ray diffraction characterization, nitrogen adsorption–desorption measurement, and transmission electron microscopy, the resulting material had an ordered mesostructure and a well-defined pore arrangement. It was applied as catalyst for the ATH of aryl-substituted α-haloketones and benzils in water affording the mono- and di-alcohols in high yields and enantioselectivities within short reaction times. In addition to its hydrophobicity and phase-transfer features, the catalyst was easy to recover by centrifugation and effectively reused for 8 consecutive ATH of 2-bromo-phenylethanone. According ICP-AES analysis, the rhodium leaching was rather low with 3.4% after 8 cycles and may explain the continuous high catalytic activities, yields and enantioselectivities.

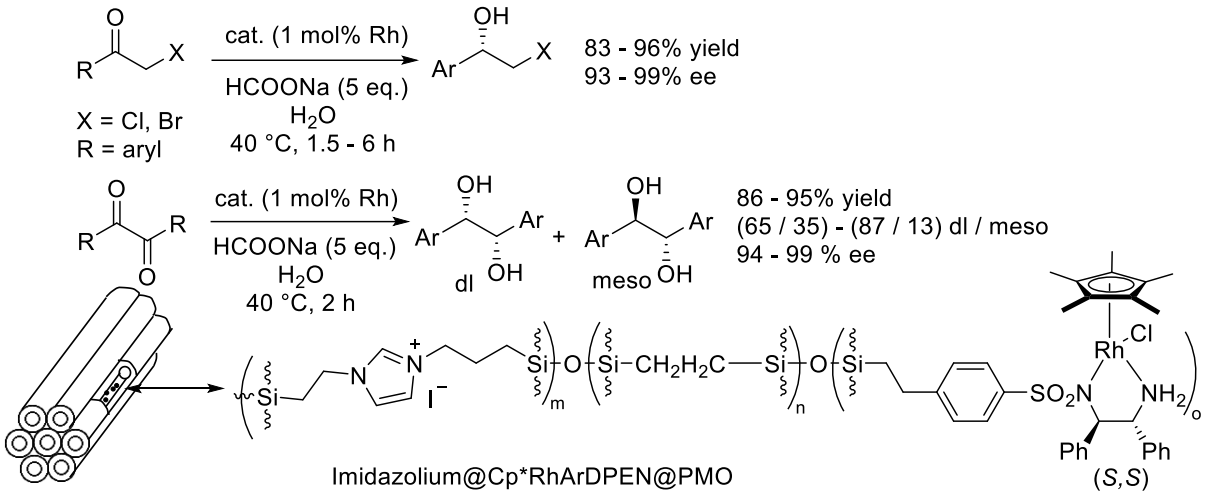

Scheme 24. ATH of α-haloketones and benzils in water with an ArDPEN-rhodium catalyst supported on a hydrophobic mesoporous organosilica. Reproduced/Adapted from Ref. [81] with permission from The Royal Society of Chemistry.

Afterwards, Yang and co-workers immobilised a DPEN–rhodiumCp* complex through encapsulation into semipermeable microporous silica nanoparticles using cross-linked polymerisation of Pickering emulsions containing octanol, styrene, divinylbenzene and the complex (Scheme 25) [82]. The resulting organic−inorganic hybrid microreactor displayed semipermeable and hydrophobic/hydrophilic properties which allowed its use in water to catalyse the ATH of small-sized ketones. The activities, conversions and enantioselectivities were good to high, similar to the homogeneous catalyst. Interestingly, a size–selectivity was noticed due to the small micropores in the silica shells (1.0−1.5 nm), allowing a good diffusion of small molecules through the microreactor and limiting or blocking the reactivity of large reactants. Upon recycling this catalyst for 5 cycles, the enantioselectivity remained stable but gradual decrease of the catalytic activity and conversions were observed. Such a deactivation process was not investigated further but longer reaction times allowed the ATH completion.

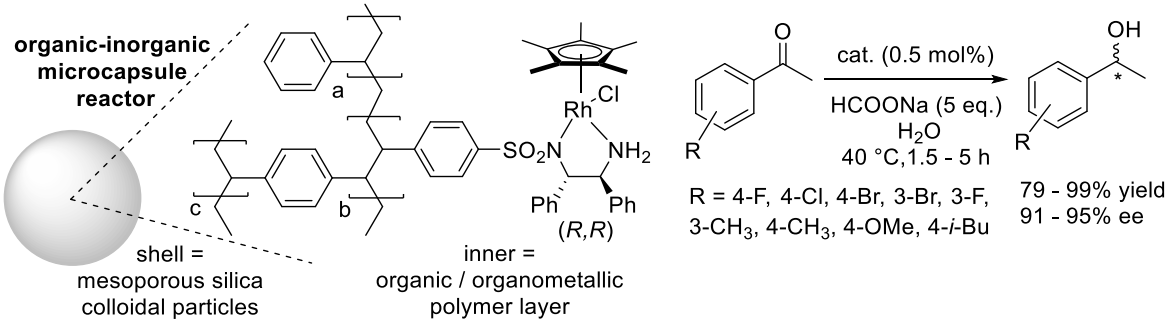

Scheme 25. ATH of ketones in water with a DPEN–rhodium catalyst supported on semipermeable and hydrophobic/hydrophilic silica nanoparticles. Reproduced/Adapted from Ref. [82] with permission from the American Chemical Society.

2.2.2. Tandem reactions

In 2017, Liu and co-workers reported a dual catalyst through the immobilisation of DABCO and a DPEN–rhodiumCp* complex on mesostructured silica nanospheres (Scheme 26) [83]. While the base was covalently bonded to the support, the organometallic complex was supported through H-bonding interaction between its BF_4 anion and the silica silanols. The resulting material was applied to catalyse an ATH–epoxidation tandem reaction, the rhodium species catalysing first the haloketone–to–haloethanol ATH and the DABCO enabling the subsequent epoxidation. Yields and enantioselectivities of epoxides were high and the catalyst was recovered by centrifugation. Though it was reused for 7 cycles affording the final epoxide in rather stable yields and enantioselectivities, a further 8th cycle resulted in a significant drop of the yield due to a rhodium leaching of 13% according ICP-AES analysis. Interestingly, chiral β-amino alcohols were also prepared in high yields and enantioselectivities using this dual catalyst through a one-pot amination–ATH tandem reaction. DABCO promoted first the synthesis of the aminoketones that were subsequently reduced by the rhodium species through ATH.

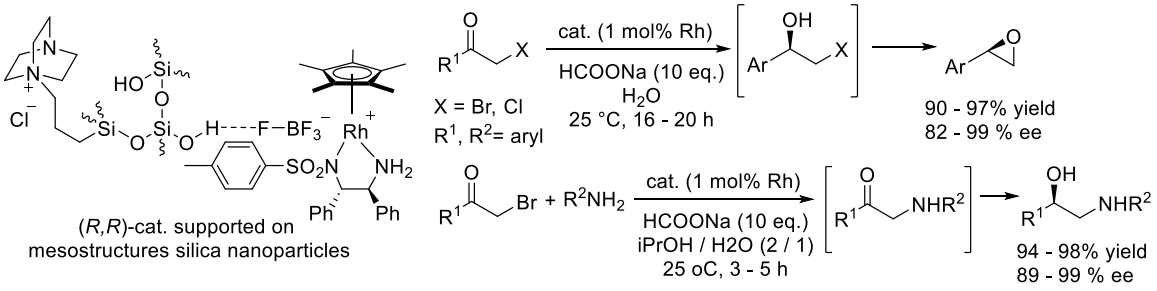

Scheme 26. Tandem ATH–epoxidation and amination–ATH with rhodium and DABCO catalysts supported on silica mesostructured nanospheres. Reproduced/Adapted from Ref. [83] with permission from Wiley-VCH.

In 2018, Liu and co-workers immobilised a DPEN–Rh–Cp* complex on a superhydrophobic mesostructured silica support and applied it to a tandem ATH–lactonisation of ethyl 2-acylarylcarboxylates (Scheme 27) [84]. Various chiral phthalides were obtained in high yields and enantioselectivities within a rather short reaction time of 5 hours thanks to the high hydrophobicity of the support and the uniform distribution of the rhodium species in the mesoporous silica as highlighted by NMR and microscopy analyses. The recycling of the catalyst was performed for 8 cycles and a small decrease of yield from 99% to 90% was observed, while the enantioselectivity remained stable. It was worth to note a similar reusable catalyst was prepared with mesitylene ruthenium DPEN and successfully applied to the ATH-DKR of α-benzoyl-β-ketophosphonates.

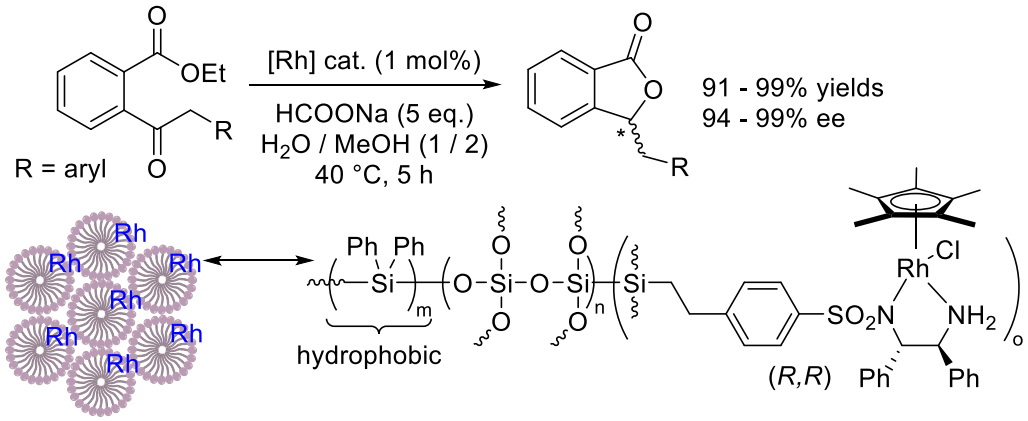

Scheme 27. Tandem ATH–lactonisation with a rhodium catalyst supported on a superhydrophobic mesostructured silica. Reproduced/Adapted from Ref. [84] with permission from The Royal Society of Chemistry.

Latter, Liu and co-workers supported 2,2,6,6-tetramethylpiperidine-1-oxyl (TEMPO) onto the outer surface of silica nanoparticles, and immobilised the DPEN–Rh–Cp* complex in the nanochannels of thermoresponsive polymer-coated hollow-shell mesoporous silica nanoparticles (Scheme 28) [85]. By integrating them into a dual catalyst system, they performed an efficient redox deracemisation of secondary alcohols in one-pot. At 0°C, the TEMPO species (cat. 1) catalysed the oxidation of racemic secondary alcohols into ketones which were reduced in situ at 40°C by the chiral DPEN–Rh–Cp* species (cat. 2) to afford the corresponding secondary alcohols in high yields and enantioselectivities. Furthermore, while studying the ATH of acetophenone, the dual catalyst was recycled for 6 cycles, with a slow decrease of yield

and enantioselectivity in (*S*)-phenylethanol, from 97% yield and 98 % ee after the first cycle to 86% yield and 90% ee after the sixth cycle. However, such deactivation process was not investigated through further analyses. Interestingly, such heterogenised dual catalyst can effectively solve the problem of mutual interactions between TEMPO and DPEN–Rh–Cp* and provide effectively various chiral alcohols by comparison to the related unsupported catalysts.

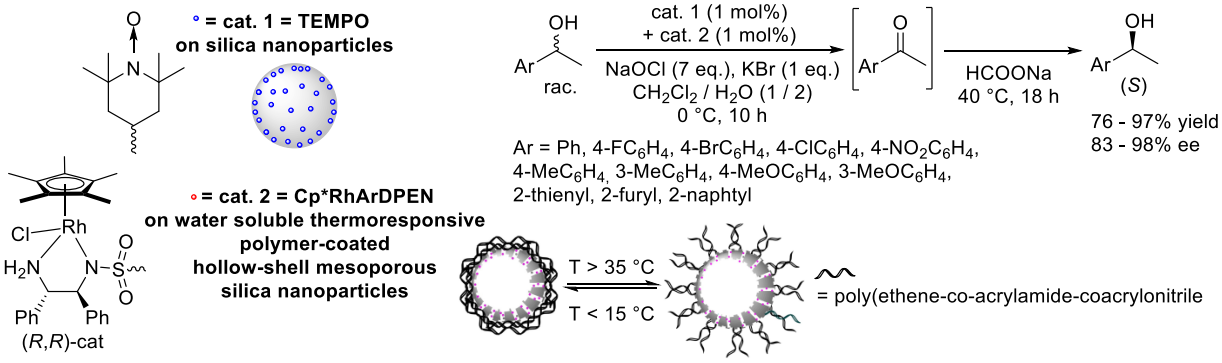

Scheme 28. Tandem oxidation–ATH with TEMPO and DPEN–Rh–Cp* catalyst supported on thermoresponsive polymer-coated hollow-shell mesoporous silica nanoparticles. Reproduced/Adapted from Ref. [85] with permission from Wiley-VCH.

2.3. Iridium based catalysts

In 2017, Itsuno and Takahashi prepared a chiral main-chain polyamide containing a (*R*,*R*)-1,2-(TsDPEN) ligand using a polycondensation method (Scheme 29) [86]. The resulting polymer chiral ligand was combined with $[IrCl_2Cp^*]_2$ and applied to the ATH of acetophenone and a cyclic sulfonimine to lead to the phenylethanol and sulfonylamine products in high yields and enantioselectivities. Noteworthy, the polymeric catalyst was separated from the organic products by a simple filtration and was reused up to 4 times. While the enantioselectivity remained stable, a gradual loss in catalytic activity was observed. By comparison, polymeric ruthenium complexes were much less active (12 h of reaction vs. 1-2 h) but led to similar enantioselectivities. Similarly, when compared to iridium catalysts, rhodium derivatives required double reaction times to afford products in high yields but lower enantioselectivities.

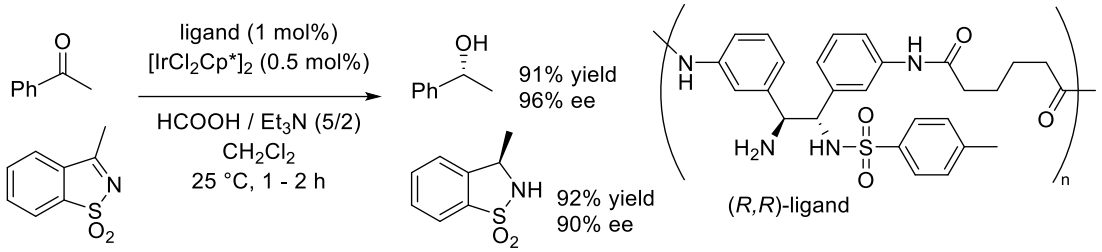

Scheme 29. ATH of imines and ketones with iridium catalyst supported on a chiral polyamide. Reproduced/Adapted from Ref. [86] with permission from Wiley-VCH.

In 2019, Blacker and co-workers reported the synthesis of a chiral iridium Cp* complex bound to (*S*,*S*,*S*)-N-camphorsulfonyl-1,2-diphenylethylene diamine (CsDPEN) and immobilised on a Wang resin (Scheme 30) [87]. They studied the ATH of various acetophenones under continuous flow mode using isopropanol as the hydrogen donor and solvent. Depending on the substrate substituents, yields and enantioselectivities were good to high. By comparison to the homogeneous catalyst, similar enantioselectivities of 94% ee were observed but the activity of the supported catalyst was much higher with a turnover number (TON) of 388 h^{-1} instead of 24 h^{-1}. Authors noticed triethylamine was the best base in order to keep high yields and ee along time. Indeed, the use of KOtBu in excess resulted in the removal of the chiral ligand and the generation of a racemic but active catalytic species. The length of the catalyst tether was also critical: the C14 chain resulted in a more active but much less stable catalyst by comparison to the C5 one, probably due to an entanglement of the tethers. Importantly, rather low levels of iridium (58–147 ppm) leaching were measured after 5 days of process.

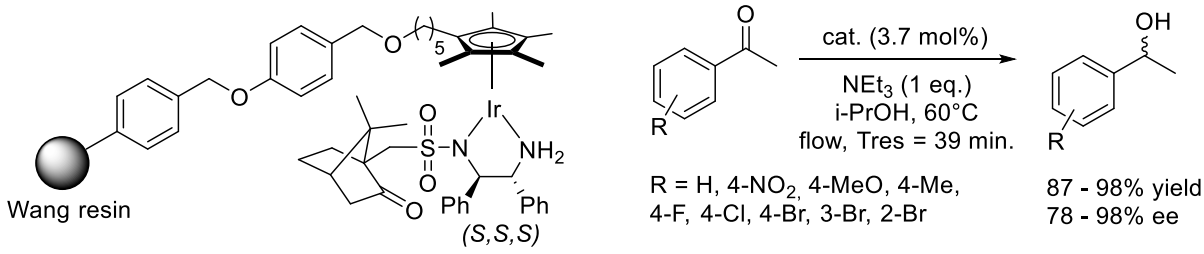

Scheme 30. ATH of ketones under continuous flow with an iridium catalyst supported on Wang resin. Reproduced/Adapted from Ref. [87] with permission from Wiley-VCH.

3. Catalysts set in ionic liquids and micelles

3.1. Ruthenium based catalysts

3.1.1. ATH

In 2015, Abu-Reziq and co-workers developed magnetically separable silica microcapsules that incorporate in their inner shell an oil-in-water emulsion with chiral ArDPEN-ruthenium catalysts and magnetic Fe_3O_4 nanocrystals coated with oleate groups (Scheme 31) [88]. The catalytic ATH of aromatic ketones proceeded in water with the use of a surfactant like cetyltrimethylammonium chloride (CTAC) in order to dissolve the organic substrates within the micelles and transfer them within the microreactors. The corresponding alcohols were obtained in high yields and good to high enantioselectivities. Thanks to its magnetic properties, the catalyst was easily recovered but a decrease of yield was noticed after the fourth run, likely due to diffusion issues, as no ruthenium leaching was detected.

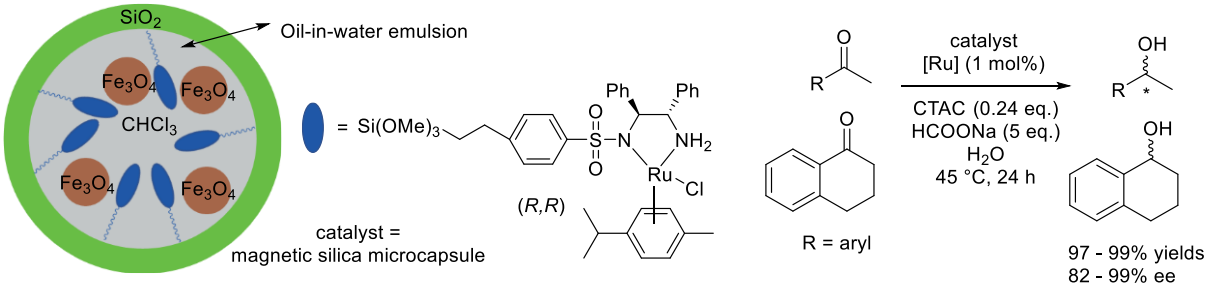

Scheme 31. ATH of ketones in water with a DPEN–ruthenium catalyst supported on magnetic mesoporous silica microcapsules. Reproduced/Adapted from Ref. [88] with permission from Wiley-VCH.

The same year, Bica and co-workers prepared chiral aminoalcohol ligands based on norephedrine and comprising a pyridinium moiety with alkyl chains of various lengths for applications in ruthenium-catalysed ATH of ketones in water (Scheme 32) [89]. The resulting alcohols were obtained with low to high yields and enantioselectivities and the length of the pyridinium alkyl chain of the ligand appeared to have no significant effect on the catalysis outcome. A recycling of the catalyst was performed on the ATH of acetophenone but a strong decrease of yields and enantioselectivities was observed over three runs suggesting a leaching or a decomposition of the catalyst that were not investigated.

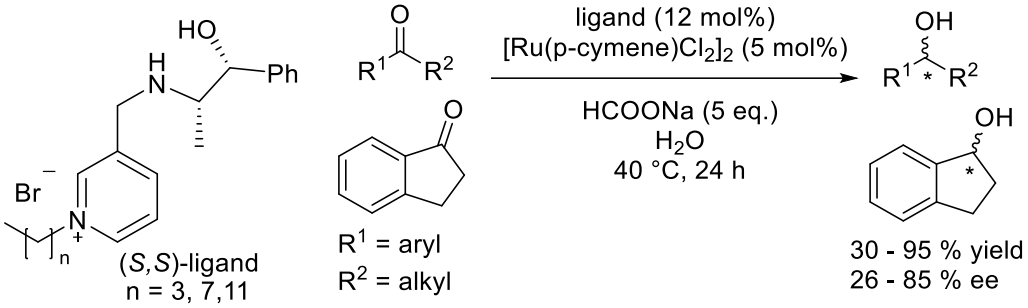

Scheme 32. ATH of ketones in water with a ruthenium catalyst supported in coordinating ionic liquids. Reproduced/Adapted from Ref. [89] with permission from Wiley-VCH.

In parallel, Nishide, Kawasaki and co-workers synthesised a series of zwitterionic ligands based on (1*S*,2*S*)-*N*-(p-toluenesulfonyl)-1,2-diphenylethylenediamine (TsDPEN) derivatives with various quaternary ammonium moieties, and applied them to the ATH of ketones in 1-butyl-3-methylimidazolium hexafluorophosphate [bmim][PF_6] ionic liquid (IL) (Scheme 33) [90]. The catalytic performances and recyclability strongly depended on the structure of the quaternary ammonium and the length of the alkyl chain linker. The ligand bearing an imidazolium group and a tetramethylene linker afforded the best conversions, enantioselectivities and reusability in the ATH of various ketones. By studying the ATH of acetophenone, the catalyst was recycled for 5 cycles, keeping the same enantioselectivity but showing a decrease of conversion at the fifth run, from 99 to 75% conversion. Nevertheless, the ruthenium content in the IL phase was superior to 99% according measurements by ICP-MS.

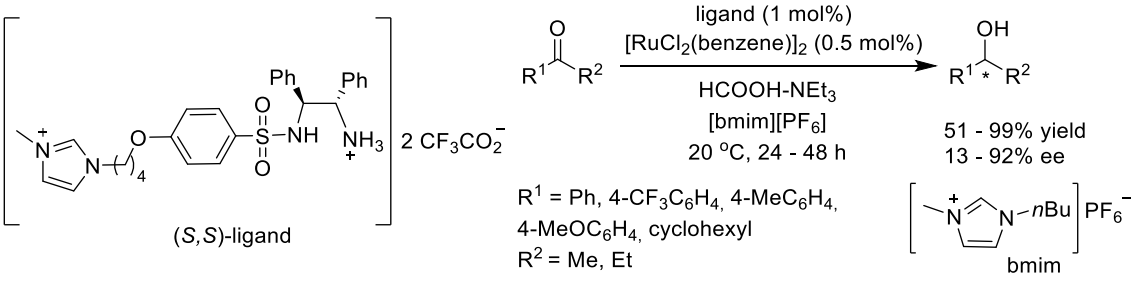

Scheme 33. ATH of ketones with a ruthenium catalyst supported in ionic liquids. Reproduced/Adapted from Ref. [90] with permission from the Pharmaceutical Society of Japan.

The same year, Hou and co-workers developed a catalyst combining a thermoregulated ionic liquid comprising a PEG-4000 fragment with arene-ruthenium complexes (Scheme 34) [91]. The latter were prepared from the combination of $[RuCl_2(p\text{–cymene})]_2$ with a mixture N-(p-tolylsulfonyl)-1,2-diphenylethylenediamine ligands sulfonated on the 4,4'-, 4,3'- and 3,3'-positions of the phenyl substituents (TsDPENDS, sodium salt). The abundances of the derivatives sulfonated on the 4,3'- and 3,3'- positions were of 23% and 76% respectively, and the one of the ligand sulfonated on the 4,4'- positions was of 2 %. The resulting mixture of organometallic complexes [PEG-4000-C_8MIM] [Ru-TsDPENDS] was applied to catalyse the ATH of aromatic ketones in ethylacetate using an HCOOH-NEt_3 azeotrope as hydrogen donor. The corresponding alcohols were obtained in fair to high conversions with high enantioselectivities. Noteworthy, the catalysts comprising C_8 alkyl chains on the methyl-imidazolium moieties were more soluble in ethylacetate than their C_1 or C_4 counterparts and led to much higher conversions. Moreover, after an ATH, the catalyst was effectively separated from the organic phase in ethyl acetate at 0°C, thanks to its thermoregulated phase-separation behavior and the total amount of ruthenium leaching into the organic phase was measured at 2.8 ppm by ICP-AES. Therefore, by studying the ATH of acetophenone, a recycling of the catalyst was performed for 5 runs and led to the same enantioselectivity but with a gradual decrease of the conversion from 98% (1st run) to 83% (5th run).

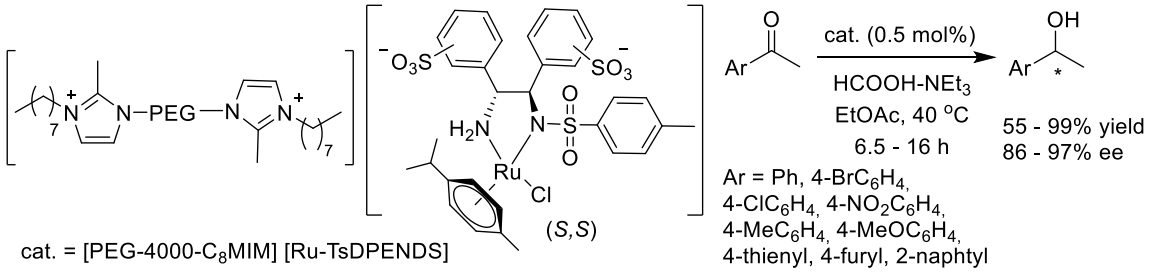

Scheme 34. ATH of ketones with a ruthenium catalyst supported in a thermoregulated ionic liquid. Reproduced/Adapted from Ref. [91] with permission from Elsevier.

Through the use of a micellar approach, Denizalti and co-workers prepared chiral amide/amine ligands prepared from L-proline and combined them with $[RuCl_2(p\text{-cymene})]_2$ to in situ generate catalysts for the ATH of aromatic ketones in the presence of sodium formiate as hydrogen donor and sodium dodecyl sulfate (SDS) as surfactant (Scheme 35) [92]. The

catalytic results revealed the best yields and enantioselectivities were obtained using a chiral proline amide ligand having a more acidic N-H moiety and bulky diisopropyl groups on the 2 and 6 positions of the phenyl substituent. The authors did not study the formation of micelles, nor the catalyst recycling, but the related organometallic complexes were synthesised and the resolution of a crystal structure by X-ray diffraction analysis indicated the ruthenium centre had a (*R*) configuration.

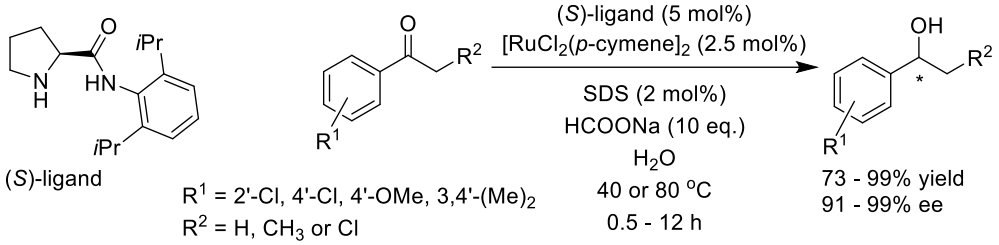

Scheme 35. ATH of ketones in water with a ruthenium catalyst within micellar conditions. Reproduced/Adapted from Ref. [92] with permission from Elsevier.

In 2019, Bica, Schröder and co-workers developed a novel chiral coordinating ionic liquid based on a diamine ligand comprising both carbamate and pyridinium moieties. Application to the ruthenium catalysed ATH of ketones in water resulted in alcohols with low to high yields and enantioselectivities (Scheme 36) [93]. Noteworthy, the ligand substituted by a dodecane alkyl chain helped in improving the ATH of alkyl ketones, the yields and ee being significantly increased. A recycling of the catalyst was performed on the ATH of acetophenone for 6 cycles. If the enantioselectivity did not vary, the conversions gradually decreased from 99 (1st run) to 82% conv. (7th run) but a possible leaching was not evidenced by any analysis.

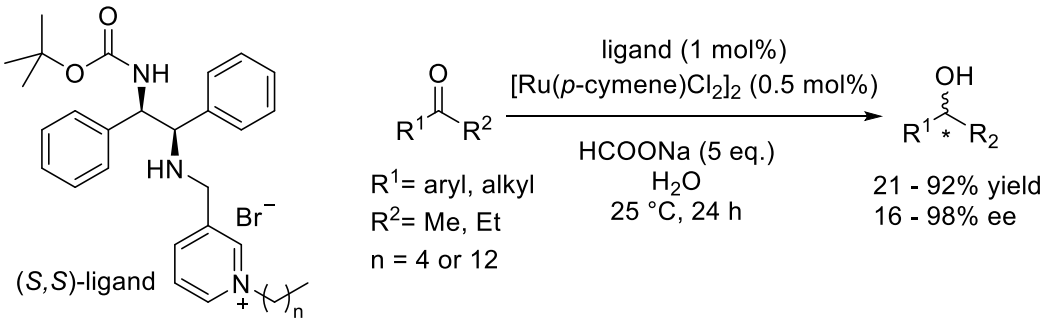

Scheme 36. ATH of ketones in water with a ruthenium catalyst in a coordinating ionic liquid. Reproduced/Adapted from Ref. [93] with permission from the American Chemical Society.

The same year, Bica-Schröder and co−workers reported that the combination of a bisulfonated−TsDPEN−ruthenium complex and a surface active ionic liquid such as $[C_{12}mim][(iC_8)_2PO_2]$ generated microemulsions that were interesting reaction media for the ATH of ketones (Scheme 37) [94]. Aromatic ketones led to the corresponding alcohols in high yields and enantioselectivities, but aliphatic derivatives were less successful. Though the microemulsions allowed for rather good reactivity and easy product separation due to their temperature-dependent phase behavior, a serious decrease of the reaction yields was observed along the recycling experiments due to the gradual decomposition of the ruthenium catalyst.

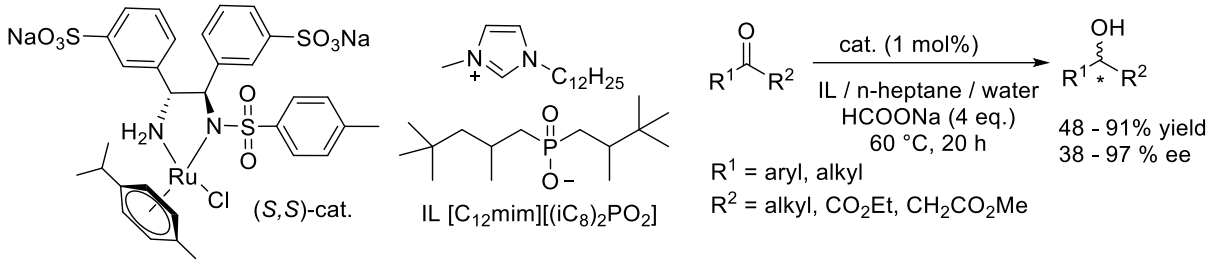

Scheme 37. ATH of ketones with a ruthenium catalyst within thermomorphic microemulsions based on ionic liquids. Reproduced/Adapted from Ref. [94] with permission from the American Chemical Society.

In 2020, Li, Jia and co-workers supported an ArDPEN ligand on a polymer issued from the co-polymerisation of N-((1*R*,2*R*)-2-amino-1,2-diphenylethyl)-4-vinylbenzenesulfonamide and methacrylic acid (Scheme 38) [95]. The complexation with $[RuCl_2(p\ cymene)]_2$ resulted in a chiral ruthenium copolymer that was combined with polymeric ionic liquids in a mixture of solvents to lead to a catalyst exhibiting a controlable hydrophobic surface and therefore amphiphilic properties thanks to the presence of chloride and NTf_2 anions. By enhancing the adsorption of organic substrates, the prepared catalyst allowed the ATH of aliphatic and aromatic ketones in water with high conversions and enantioselectivities. Interestingly, the catalyst was recovered through a simple extraction and recycled for nine runs with only a minor decrease of activity and enantioselectivity due to a small ruthenium leaching of 3.4% according ICP–AES analysis.

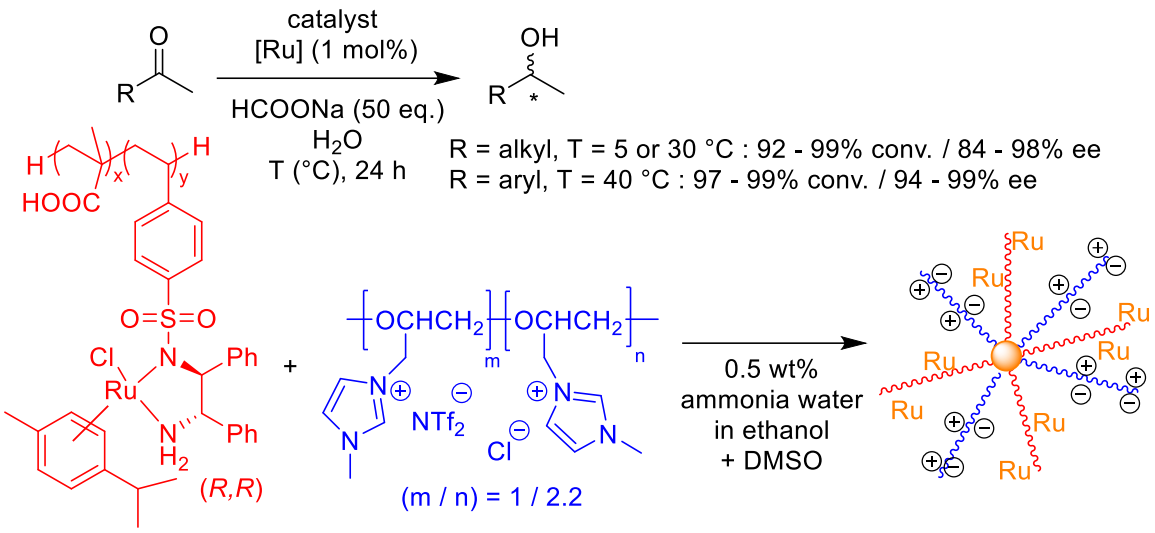

Scheme 38. ATH of ketones in water with a ruthenium catalyst in polymeric ionic liquid. Reproduced/Adapted from Ref. [95] with permission from the American Chemical Society.

3.1.2. Tandem reactions

In 2016, Chen, Wu and co-workers studied the application of amino-alcohol ligands based on chloramphenicol to the ruthenium catalysed ATH and DKR of various N–Boc–α–amino–β–ketoesters to afford anti–N–Boc–β–hydroxy–α–amino esters with fair to high yields, diastereoselectivities and enantioselectivities (Scheme 39) [96]. The catalytic process implied the use of water as solvent and polyethylene glycol sorbitan monolaurate, Tween 20, as surfactant, but the authors did not studied the formation of micelles, nor the catalyst recycling. Finally, such ATH was successfully applied to the stereoselective synthesis of a key building block of the antibiotic vancomycin.

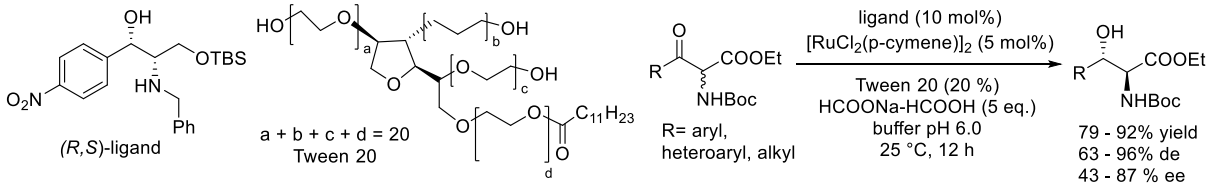

Scheme 39. ATH and DKR of N-Boc α–amino-β-ketoesters in water with a ruthenium catalyst within micellar conditions. Reproduced/Adapted from Ref. [96] with permission from The Royal Society of Chemistry.

3.2. Rhodium based catalysts

3.2.1. ATH

Through the combined use of a surfactant-type TsDPEN ligand and $[RhCl_2Cp^*]_2$, Deng and co-workers reported a rhodium catalysed ATH of ketoeters and acyloxyketones in water (Scheme 40) [97]. Except for some specific substrates, the reduced products were recovered in high conversions and enantioselectivities provided that parameters like the temperature, the pH and the volume, as well as the alkyl chain length of the aliphatic ketoesters or of the surfactant-type ligand were controled. The observed spherical metallomicelles had indeed a significant impact on the catalytic activity and enantioselectivity. Thus, on their surface, electrostatic attractions between the positive polar heads of the surfactants and the formate ions resulted in an acceleration of the reaction rate. Moreover, within the metallomicelle core, steric hindrance, CH/π interactions and strong hydrophobic interactions between the catalyst and the substrate played a key role in the catalytic transition state and the asymmetric induction.

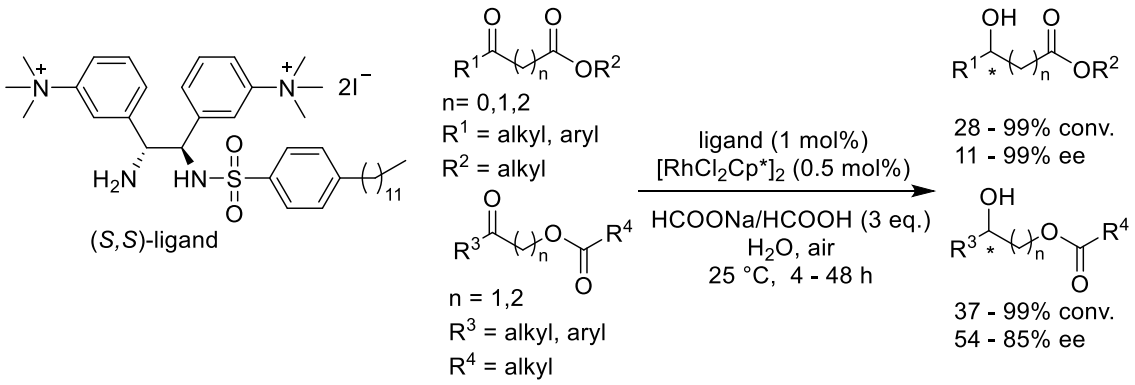

Scheme 40. ATH of ketoeters and acyloxyketones in water with a rhodium catalyst within micellar conditions. Reproduced/Adapted from Ref. [97] with permission from the American Chemical Society.

Afterwards, Deng and co-workers developed other surfactant-type TsDPEN ligands for the rhodium catalysed ATH of various organic compounds in water (Scheme 41) [98]. Whereas the rhodium complex of the ligand substituted by a single alkyl chain on the sulfonyl aryl ring was self-assembled into spherical micelle particles, the rhodium complex of the ligand functionalised by a double alkyl chain resulted in vesicular aggregates formed of a bilayer and a hollow core (Scheme 41). Interestingly, the latter displayed enhanced activities and

enantioselectivities for the ATH of ketones and β-ketoesters by comparison to the spherical micelles obtained with the single alkyl chain TsDPEN ligand. Moreover, application to the DKR of bicyclic β-ketoesters was also effective. TEM analyses indicated that the formed vesicles had nearly ten times the diameter of the spherical micelles and therefore suggested the bilayer formed from these vesicles significantly enlarged the interfacial area of the catalyst layer and contributed to the higher catalytic activity. Indeed, this implied higher solubilities and concentrations of the HCOONa hydrogen source in the hydrophilic parts and of the organic substrates in the hydrophobic domains, the latter being enhanced by the lipophilic double alkyl chains.

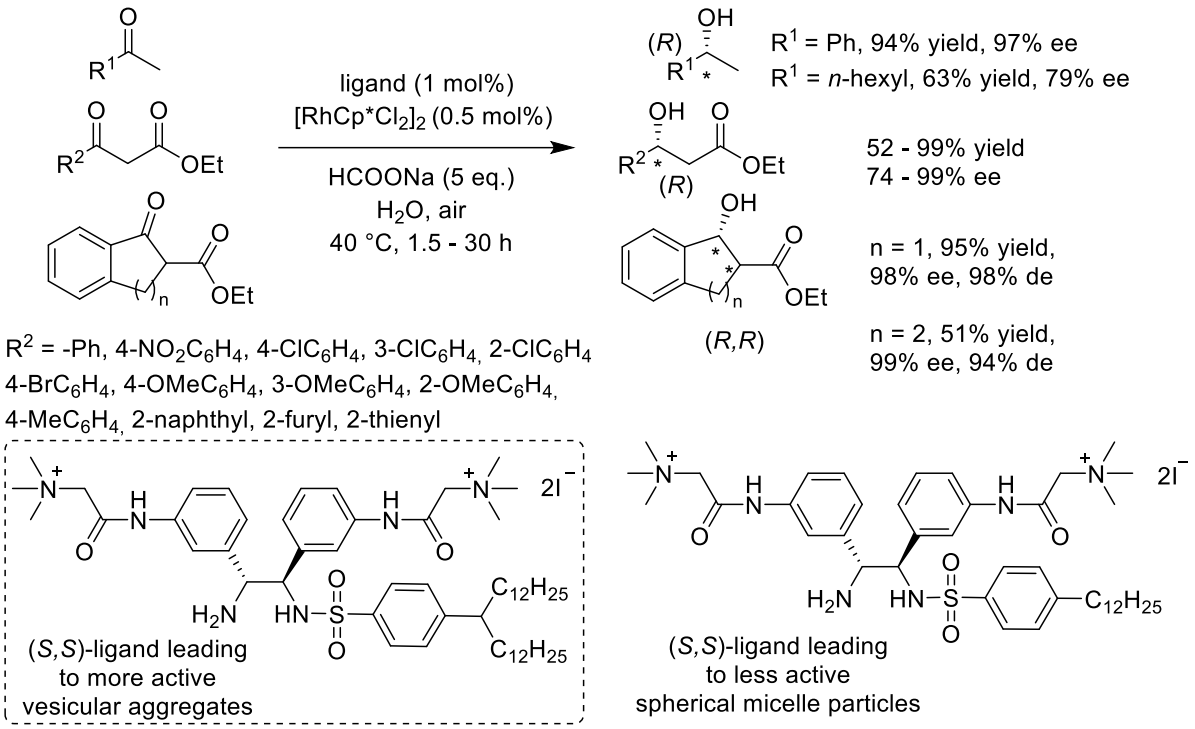

Scheme 41. ATH of arylketoesters in water with a chiral surfactant-type diamine ligand and $[RhCl_2Cp^*]_2$. Reproduced/Adapted from Ref. [98] with permission from The Royal Society of Chemistry.

In 2019, Vidal and co-workers prepared a tethered rhodium(III) catalyst based on an electron-deficient diamine ligand carrying a pentafluorobenzenesulfonyl substituent for application to a DKR–ATH of α-methoxy-β-keto esters (Scheme 42) [99]. The reaction proceeded in water without any co-solvent, thanks to the use of a sub-stoichiometric amount of

cetyltrimethylammonium bromide (CTAB) as surfactant which outperformed sodium dodecyl sulfate (SDS). Monodifferentiated β-hydroxyester derivatives were obtained in high yields (up to 98%) with high levels of diastereoselectivity (up to >99:1) and excellent ee values (up to >99%) on 0.6 to 6 mmol scales. However, the authors did not studied the catalyst recycling, nor the formation of micelles.

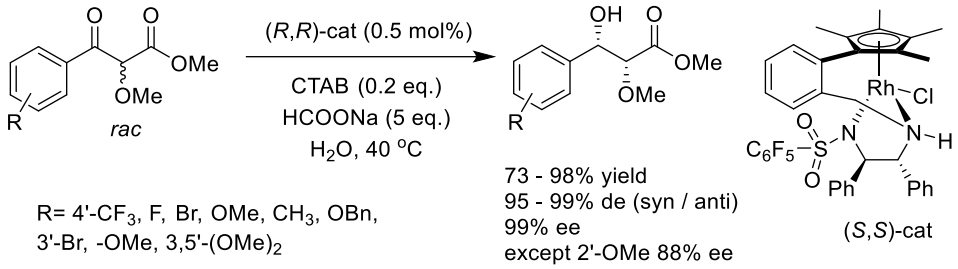

Scheme 42. ATH of α-methoxy β-ketoesters in water with rhodium catalyst within micellar conditions. Reproduced/Adapted from Ref. [99] with permission from Wiley-VCH.

The same year, Li, Deng and co-workers applied a chiral surfactant-type diamine ligand for the rhodium catalysed ATH of ketones in water (Scheme 43) [100]. Several parameters influenced the activity and the enantioselectivity of the catalytic system including the length of the ligand aliphatic tail, the concentration of catalyst, and the nature of the solvent. Aliphatic ketones as well as α,β-unsaturated ketones were reduced to the corresponding aliphatic alcohols in high conversions and enantioselectivities. The authors showed the good performances of the chiral surfactant-type catalytic system were related to the length of the catalyst alkyl chain, the latter affecting the size and structure of the formed micelle aggregates. Indeed, the longer the catalyst alkyl chain was, the smaller and more regular the spherical micelles were and the better the catalysis results were. The molecular structure of the substrates had also a significant influence on the catalysis outcome.

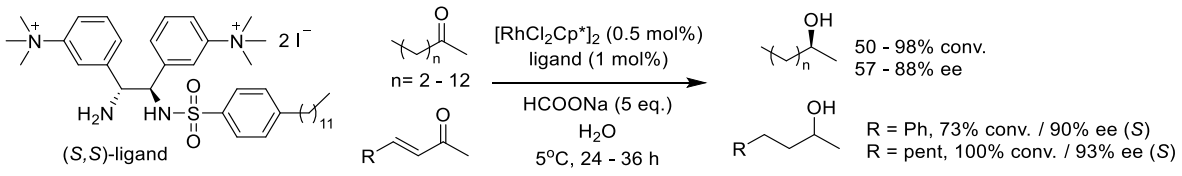

Scheme 43. ATH of ketones in water with a rhodium catalyst comprising a chiral surfactant-type diamine ligand. Reproduced/Adapted from Ref. [100] with permission from Elsevier.

In 2022, Weck and co-workers reported an example of photoresponsive nanoreactor for substrate-selective ATH by using an azobenzene derivative as a photoresponsive cross-linking agent (Scheme 44) [101]. Under visible light, the trans isomers of azobenzene units led to a hydrophobic cross-linked layer which prevented the diffusion of the hydrogen donor HCOONa and therefore any catalysis. In contrast, upon UV light irradiation, the cis isomers of azobenzene allowed an increase in polarity and hydrophilicity, and therefore the diffusion of HCOONa to the micelle core and the Rh-TsDPEN catalyst, with the micelles hydrodynamic diameter switching from about 81 nm to 60 - 68 nm. Kinetic studies of the ATH confirmed such a discrimination for the hydrogen donor reagent, as well as for substrates, smaller aromatic ketones reacting faster within the nanoreactor under UV irradiation. The corresponding alcohols were recovered in fair to high yields and high enantioselectivities even after 3 cycles.

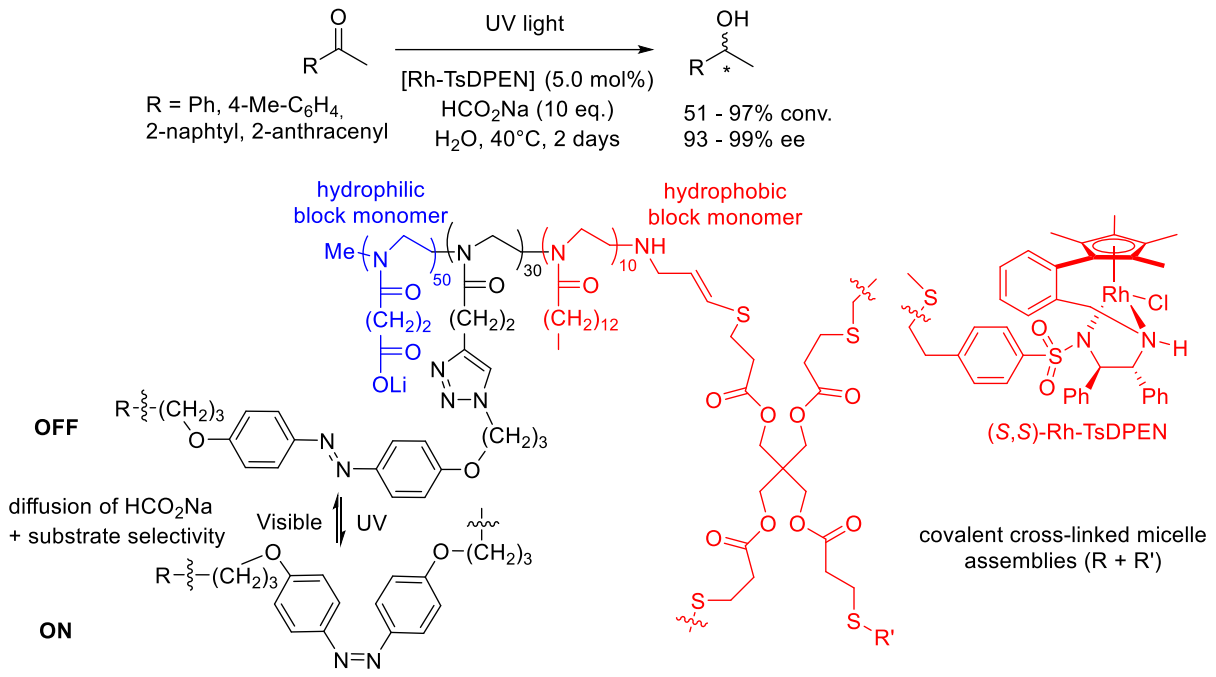

Scheme 44. ATH of ketones in water with a rhodium catalyst supported in photoregulated covalent cross-linked micelles. Reproduced/Adapted from Ref. [101] with permission from the American Chemical Society.

3.2.2. Tandem reactions

In 2015, Weck and co-workers developed a two-step catalytic tandem reaction in water implying a cobalt(III) catalysed hydration of alkynes and a rhodium(III) catalysed ATH of the

resulting ketones (Scheme 45) [102]. The cobalt porphyrin and rhodium-TsDPEN catalysts were immobilised in the multicompartmentalised domains of a core−shell cross-linked micelle. The catalytic tandem proceeded in one pot leading first to the alkyne hydration and the ATH of the resulting ketones afforded the related alcohols with high conversions and enantioselectivities. Although the tandem reaction worked with the two catalysts immobilised on different micelles, the multicompartmentalised micelle containing both catalysts gave better results, thanks to the optimal microenvironments provided for each catalytic reaction and to the intramicellar diffusion of the ketone intermediate. Though the nanocatalyst recycling was not studied and the functionalised domains available within a micelle may limit the possible catalytic steps, the developed nanoreactor allowed tandem reactions involving incompatible catalytic transformations.

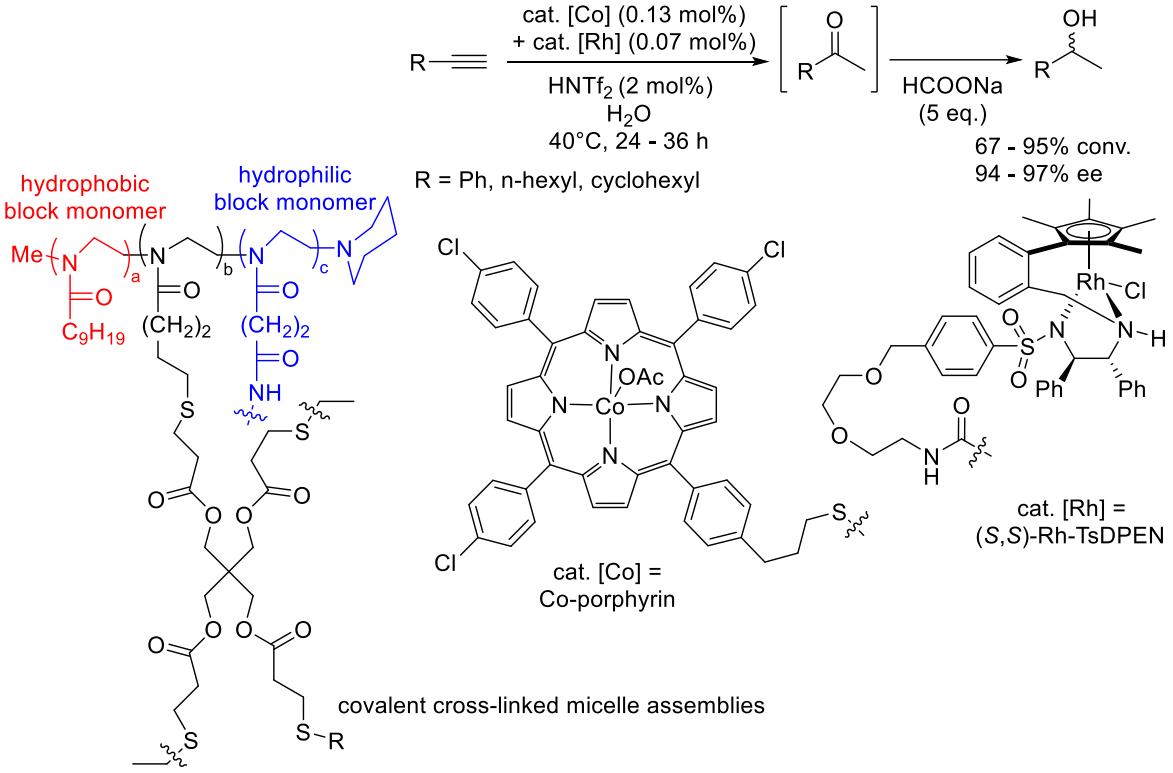

Scheme 45. Tandem hydration−ATH in water with cobalt and rhodium catalysts supported in core-shell cross-linked micelles. Reproduced/Adapted from Ref. [102] with permission from the American Chemical Society.

Latter, Weck and co-workers reported a compartmentalisable nanoreactor which was organised in spherical micelles and allowed a three-step, non-orthogonal tandem reaction in one pot (Scheme 46) [103]. First, the starting ketals were hydrolysed to the corresponding ketones through an acid catalysis within the hydrophilic corona of the nanoreactor. Then, a Rh-catalysed ATH in the cross-linked shell afforded the corresponding enantio-enriched alcohols which were finally acylated through base-catalysis in the nanoreactor hydrophobic core. Though the achieved enantioselectivities were high, the conversions were low to good, depending on the substrate structure, and the recycling of the nanocatalyst was not studied. Noteworthy, the three catalysts were confined in amphiphilic poly(2-oxazoline)-based triblock copolymers that assemble into shell cross-linked micelles and were placed at critical locations, affording a good proximity to each other as well as specific microenvironments. Indeed, the intermediate shell cross-linked layer proved to prevent deactivation of the DMAP catalyst.

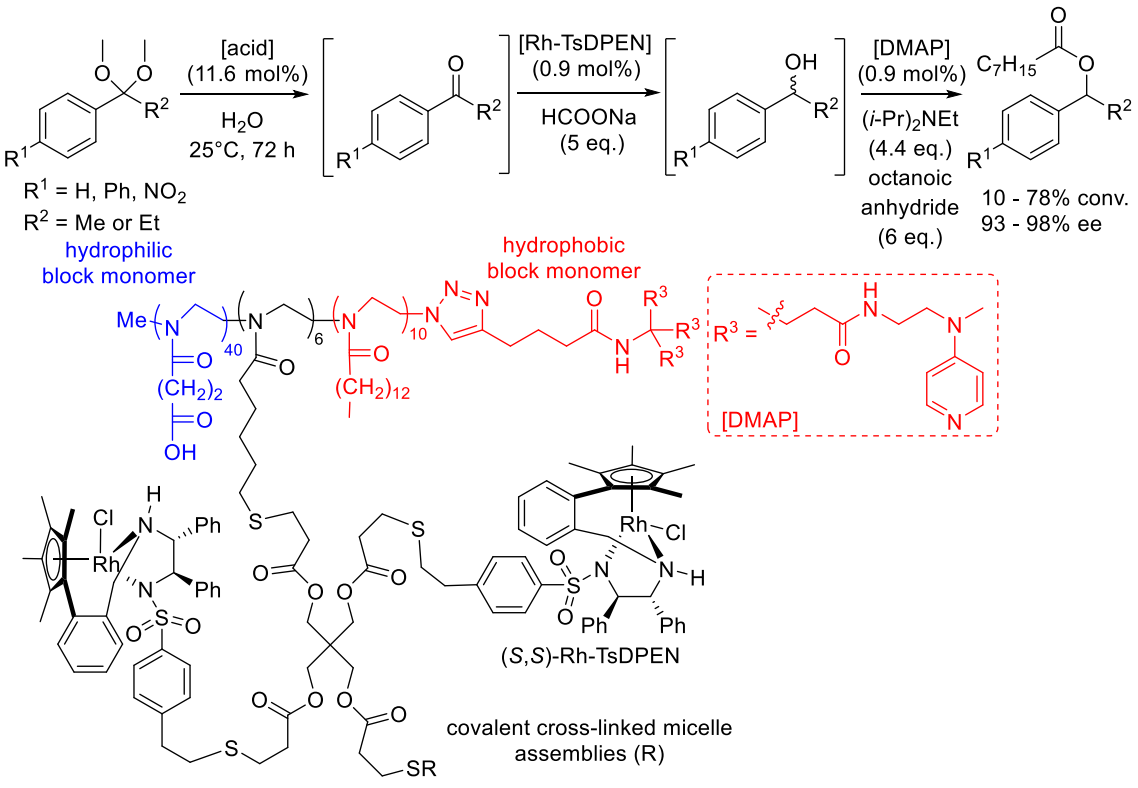

Scheme 46. Tandem hydrolysis–ATH–acylation in water with acid, rhodium and DMAP catalysts supported in shell cross-linked micelles. Reproduced/Adapted from Ref. [103] with permission from Wiley-VCH.

In 2021, Weck and co-workers developed another two-step catalytic tandem reaction in water by combining in a nanoreactor based on a core−shell micellar nanostructure, a rhodium−diene complex catalysing an asymmetric 1,4-addition with a Rh-TsDPEN complex catalysing the ATH of the resulting ketones (Scheme 47) [104]. Interestingly, the multifunctional amphiphilic poly(2-oxazolines) was covalently cross-linked with spiropyran, a photoactive molecule which could be reversibly converted to zwitterionic merocyanine upon irradiation. Thanks to this photoinduced property, the cross-linking domain allowed an effective control of the diffusion of the hydrogen donor HCOONa into the hydrophobic core of the nanoreactor. In one pot, the asymmetric 1,4-addition was first performed in the hydrophilic corona under visible light and then, upon subsequent UV irradiation, the ATH proceeded in the hydrophobic core of the nanoreactor, thanks to the photo-induced diffusion of the hydrogen donor. The catalytic tandem reactions implied different conjugated ketones and boronic acids and led to the corresponding alcohols in high conversions and enantioselectivities, but the catalyses were run under an argon atmosphere and the recycling of such nanocatalyst was not studied.

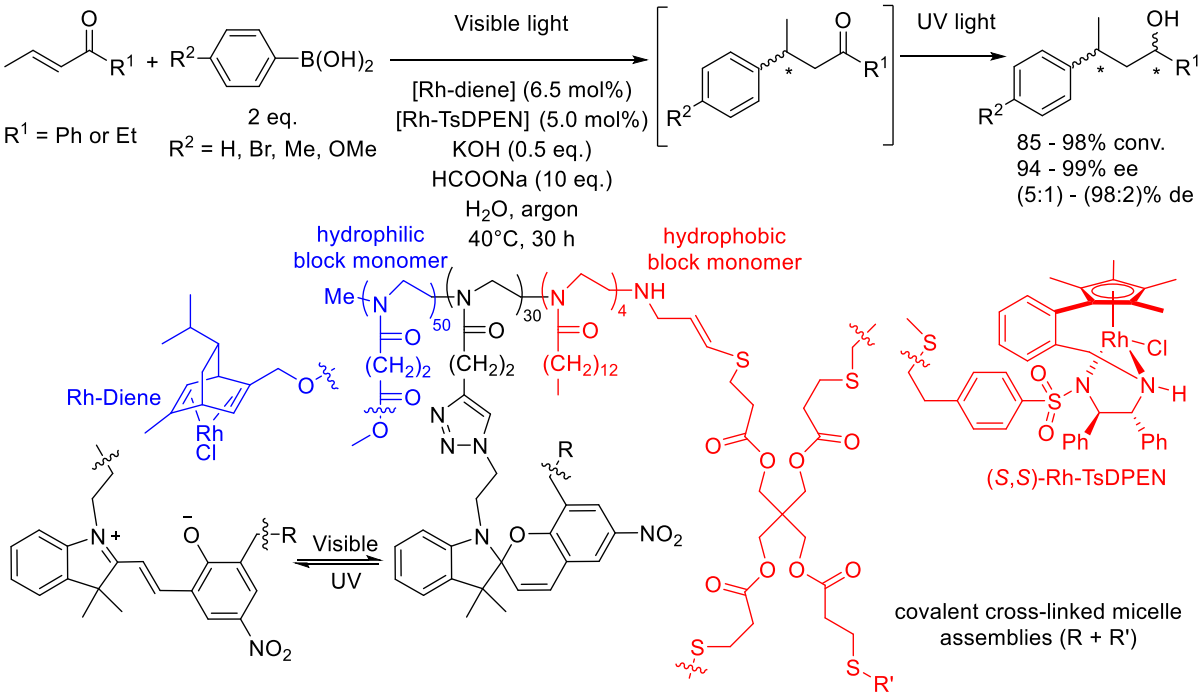

Scheme 47. Tandem 1,4-addition−ATH in water with rhodium catalysts supported in a photoregulated core−shell micellar nanostructure. Reproduced/Adapted from Ref. [104] with permission from the American Chemical Society.

3.3. Iridium based catalysts

In 2015, Deng and co-workers reported surfactant-type TsDPEN ligands for the iridium and rhodium catalysed ATH of ketoeters and acyloxyketones in water (Scheme 40) [97]. By comparison to rhodium, iridium catalysts provided lower enantioselectivities.

4. Conclusion

We have seen that the application of supported bifunctional catalysts to ATH and related tandem reactions is blooming. New examples implying ruthenium, rhodium and iridium have appeared thanks to ligand modifications and the use of different supports. Overall, the resulting catalysts performed well in the ATH of ketones and imines with fair reusabilities. These catalysts have also been combined with other supported organometallic or organic catalyst to perform effectively tandem reactions combining ATH with Sonogashira or Suzuki cross-couplings, aza-Michael reaction, alkyne hydration, lactonisation, oxysulfonylation or oxidation. Finally, an interesting perspective for industrial applications has been drawn by the use of some supported bifunctional catalysts in continuous flow[71,79,87]. Nevertheless, though these recoverable catalysts hydrogenate with high selectivities carbonyl and imine substrates, new effective hydrogenation catalysts are needed in order to reduce more challenging substrates[48] like carbocyclic arenes[105,106], nitrogen based heterocycles[107] and tri- or tetra-substituted alkenes[108,109]. In this context, the development of new chemoselective supported catalysts allowing ATH or AH[110,111] and further applications in continuous flow[112-115] may be an interesting perspective. Moreover, due to economic, environmental and societal issues, the growing interest in hydrogenation and transfer hydrogenation catalysts based on abundant metals[116-119] shall result in the development of other supported catalysts. Finally, industrial applications[120,121] will privilege the development of highly active catalysts, i.e. high turnover number catalysts, as well as applications in flow chemistry[115].

Declaration of Competing Interest

The authors declare that they have no known competing financial interests or personal relationships that could have appeared to influence the work reported in this paper.

Acknowledgments

The CNRS and the University of Strasbourg are acknowledged for supporting and funding partially this work. The University of Strasbourg and the French national program “Investment

for the future" (IdEx-Unistra 2019) are thanked for a PhD fellowship (H.P.). This work has also benefitted from support provided by the University of Strasbourg Institute for Advanced Study (USIAS) for a Fellowship to C.M, within the French national program "Investment for the future" (IdEx-Unistra 2021).

References

[1] R. Noyori, In Asymmetric Catalysis In Organic Synthesis, chapter 2, Wiley, New York, 1994.

[2] T. Ohkuma, M. Kitamura, R. Noyori, In Catalytic Asymmetric Synthesis 2nd Edition; I. Ojima, Ed.; Wiley-VCH, 2000, p 1.

[3] H.-U. Blaser, H.-J. Federsel, Eds. In Asymmetric Catalysis on Industrial Scale; Wiley-VCH, 2010.

[4] W.S. Knowles, Angew. Chem. Int. Ed. 41 (2002) 1998−2007.

[5] R. Noyori, Angew. Chem. Int. Ed. 41 (2002) 2008–2022.

[6] R. Noyori, Adv. Synth. Catal. 345 (2003) 15−32.

[7] H.U. Blaser, B. Pugin, F. Spindler, L.A. Saudan, Hydrogenation. In Applied Homogeneous Catalysis with Organometallic Compounds 3rd Edition, Wiley-VCH, 2018, 2, pp. 621−690.

[8] F. Foubelo, C. Najera, M. Yus, Tetrahedron Asym. 26 (2015) 769−790.

[9] H.G. Nedden, A. Zanotti-Gerosa, M. Wills, Chem. Record 16 (2016) 2619−2639.

[10] B. Stefane, F. Pozgan, Top. Curr. Chem. 374 (2016) 1−67.

[11] D. Wang, D. Astruc, Chem. Rev. 115 (2015) 6621−6686.

[12] A. Matsunami, Y. Kayaki, Tetrahedron Lett. 59 (2018) 504−513.

[13] E. Baráth, Catalysts 8 (2018) 671.

[14] P. Etayo, A. Vidal-Ferran, Chem. Soc. Rev. 42 (2013) 728−754.

[15] T. Ohkuma, R. Noyori, Angew. Chem. Int. Ed. 40 (2001) 40–73.

[16] T. Ohkuma, H. Ooka, S. Hashiguchi, T. Ikariya, R. Noyori, J. Am. Chem. Soc. 117 (1995) 2675–2676.

[17] R. Noyori, S. Hashiguchi, Acc. Chem. Res. 30 (1997) 97−102.

[18] S. Hashiguchi, A. Fujii, J. Takehara, T. Ikariya, R. Noyori, J. Am. Chem. Soc. 117 (1995) 7562–7563.

[19] H. Doucet, T. Ohkuma, K. Murata, T. Yokozawa, M. Kozawa, E. Katayama, A.F. England, T. Ikariya, R. Noyori, Angew. Chem. Int. Ed. 37 (1998) 1703–1707.

[20] T. Ohkuma, M. Koizumi, K. Muñiz, G. Hilt, C. Kabuto, R. Noyori, J. Am. Chem. Soc. 124 (2002) 6508–6509.

[21] C.A. Sandoval, T. Ohkuma, K. Muñiz, R. Noyori, J. Am. Chem. Soc. 125 (2003) 13490–13503

[22] K.-J. Haack, S. Hashiguchi, A. Fujii, T. Ikariya, R. Noyori, Angew. Chem. Int. Ed. 36 (1997) 285–288

[23] M.J. Palmer, M. Wills, Tetrahedron Asym. 10 (1999) 2045−2061.

[24] S. Clamham, A. Hadzovic, R.H. Morris, Coord. Chem. Rev. 248 (2004) 2201–2237.

[25] T. Ikariya, K. Murata, R. Noyori, Org. Biomol. Chem. 4 (2006) 393–406.

[26] T. Ikariya, A.J. Blacker, Acc. Chem. Res. 40 (2007) 1300–1308.

[27] C.P. Casey, J.B. Johnson, J. Org. Chem. 68 (2003) 1998–2001.

[28] D.A. Alonso, P. Brandt, S.J.M. Nordin, P. G. Andersson, J. Am. Chem. Soc. 121 (1999) 9580–9588.

[29] M. Yamakawa, H. Ito, R. Noyori, J. Am. Chem. Soc. 122 (2000) 1466–1478.

[30] S.M. Joseph, J.S. Samec, J.-E. Bäckvall, P.G. Andersson, P. Brandt, Chem. Soc. Rev. 35 (2006) 237–248.

[31] M. Sawamura, Y. Ito, Chem. Rev. 92 (1992) 857–871.

[32] H. Steinhagen, G. Helmchen, Angew. Chem. Int. Ed. 35 (1996) 2339–2342.

[33] M. Shibasaki, H. Sasai, T. Arai, Angew. Chem. Int. Ed. 36 (1997) 1236–1256.

[34] E.K. Van den Beuken, B.L. Feringa, Tetrahedron 54 (1998) 12985–13011.

[35] G. J. Rowlands, Tetrahedron 57 (2001) 1865–1882.

[36] H. Gröger, Chem. Eur. J. 7 (2001) 5246–5251.

[37] M. Shibasaki, N. Yoshikawa, Chem. Rev. 102 (2002) 2187–2209.

[38] J.-A. Ma, D. Cahard, Angew. Chem. Int. Ed. 43 (2004) 4566–4583.

[39] J. Hannedouche, G.J. Clarkson, M. Wills, J. Am. Chem. Soc. 126 (2004) 986–987.

[40] A.M. Hayes, D.J. Morris, G.J. Clarkson, M. Wills, J. Am. Chem. Soc. 127 (2005) 7318–7319.

[41] D.J. Morris, A.M. Hayes, M. Wills, J. Org. Chem. 71 (2006) 7035–7044.

[42] D.S. Matharu, D.J. Morris, A.M. Kawamoto, G.J. Clarkson, M. Wills, Org. Lett. 7 (2005) 5489–5491.

[43] R. Guo, C. Elpelt, X. Chen, D. Song, R.H. Morris, Chem. Commun. 2005 (2005) 3050–3052.

[44] R. Guo, X. Chen, C. Elpelt, D. Song, R.H. Morris, Org. Lett. 7 (2005) 1757–1759.

[45] V. Ritleng, J. G. de Vries, Molecules 26 (2021) 4076-4121.

[46] V. Ritleng, C. Michon, Molecules 27 (2022) 4703-4734.

[47] C. Michon, F. Agbossou-Niedercorn in Topics in Enantioselective Catalysis, Recent Achievements and Future Challenges, World Scientific, Series on Chemistry, Energy and the Environment, 2022, chapter 9, pp 281-367.
[48] C.S.G. Seo, R.H. Morris, Organometallics 38 (2019) 47−65.
[49] T. Ikariya, Y. Kayaki, Pure Appl. Chem. 86 (2014) 933−943.
[50] X.-Q. Dong, Q. Zhao, P. Li, C. Chen, X. Zhang, Org. Chem. Front. 2 (2015) 1425−1431.
[51] I. V. Gridnev, ChemCatChem 8 (2016) 3463−3465.
[52] J. Zhang, J. Jia, X. Zeng, Y. Wang, Z. Zhang, I.D. Gridnev, W. Zhang, Angew. Chem. Int. Ed. 58 (2019) 11505−11512.
[53] J. Chen, I.D. Gridnev, iScience 23 (2020) 100960.
[54] T. Cheng, Q. Zhao, D. Zhang, G. Liu, Green Chem. 17 (2015) 2100-2122.
[55] R.B.N. Baig, M.N. Nadagouda, R.S. Varma, Coord. Chem. Rev. 287 (2015) 137-156.
[56] Y. Wei, X. Wu, C. Wang, J. Xiao, Catal. Today 247 (2015) 104-116.
[57] B. Altava, M.I. Burguete, E. García-Verdugo, S.V. Luis, Chem. Soc. Rev. 47 (2018) 2722-2771.
[58] S. M. Sarkar, M. M. Yusoff, M. L. Rahman, J. Chin. Chem. Soc. 62 (2015) 177-181.
[59] K. Zhang, J. An, Y. Su, J. Zhang, Z. Wang, T. Cheng, G. Liu, ACS Catal. 6 (2016) 6229-6235.
[60] Y. Xie, M. Wang, X. Wu, C. Chen, W. Ma, Q. Dong, M. Yuan, Z. Hou, ChemPlusChem 81 (2016) 541-549.
[61] C. M. Eichenseer, B. Kastl, M. A. Pericas, P. R. Hanson, O. Reiser, ACS Sustain. Chem. Engineer. 4 (2016) 2698-2705.
[62] J. Canivet, E. Bernoud, J. Bonnefoy, A. Legrand, T.K. Todorova, A.E. Quadrelli, C. Mellot-Draznieks, Chem. Sci. 11 (2020) 8800-8808.
[63] S. Doherty, J.G. Knight, H. Alshaikh, J. Wilson, P.G. Waddell, C. Wills, C.M. Dixon, Eur. J. Inorg. Chem. 2021 (2021) 226-235.
[64] X. Li, J. Dong, G. Ma, N. Ma, X. Jia, J. Catal. 411 (2022) 84–92.
[65] J. Xu, T. Cheng, K. Zhang, Z. Wang, G. Liu, Chem. Commun. 52 (2016) 6005-6008.
[66] J. Wang, L. Wu, X. Hu, R. Liu, R. Jin, G. Liu, Catal. Sci. Technol. 7 (2017) 4444-4450.
[67] Y. Zhao, R. Jin, Y. Chou, Y. Li, J. Lin, G. Liu, RSC Adv. 7 (2017) 22592-22598.
[68] X. Xia, J. Meng, H. Wu, T. Cheng, G. Liu, Chem. Commun. 53 (2017) 1638-1641.
[69] L. Li, D. Yang, Z. Zhao, Y. Song, L. Zhao, R. Liu, G. Liu, Front. Chem. 6 (2018) 272.
[70] Y. Su, F. Chang, R. Jin, R. Liu, G. Liu, Green Chem. 20 (2018) 5397-5404.
[71] L. Wu, Y. Li, J. Meng, R. Jin, J. Lin, G. Liu, ChemPlusChem 83 (2018) 861-867.

[72] X. Shu, R. Jin, Z. Zhao, T. Cheng, G. Liu, Chem. Commun. 54 (2018) 13244-13247.
[73] G. Zhang, R. Liu, Y. Chou, Y. Wang, T. Cheng, G. Liu, ChemCatChem 10 (2018) 1882-1888.
[74] Z. Zhao, F. Chang, T. Wang, L. Wang, L. Zhao, C. Peng, G. Liu, Chem. Commun. 55 (2019) 13578-13581.
[75] J. Meng, F. Chang, Y. Su, R. Liu, T. Cheng, G. Liu, ACS Catal. 9 (2019) 8693-8701.
[76] M. Gao, F. Chang, S. Wang, Z. Liu, Z. Zhao, G. Liu, J. Catal. 376 (2019) 191-197.
[77] Y. Li, C. Wang, Q. Chen, H. Li, Y. Su, T. Cheng, G. Liu, C. Tan, Chem. Asian J. 16 (2021), 2338-2345.
[78] Z. Liu, Y. Wang, K. Liu, S. Wang, H. Liao, Y. Zhu, B. Hou, C. Tan, G. Liu, Front. Chem. 9 (2021) 732542.
[79] S. Wang, C. Wang, N. Lv, C. Tan, T. Cheng, G. Liu, ChemCatChem 13 (2021) 909-915.
[80] X. Zhang, Y. Zhao, J. Peng, Q. Yang, Green Chem. 17 (2015) 1899-1906.
[81] F. Zhou, X. Hu, M. Gao, T. Cheng, G. Liu, Green Chem. 18 (2016) 5651-5657.
[82] X. Zhang, L. Jing, L. Wei, F. Zhang, H. Yang, ACS Catal. 7 (2017) 6711-6718.
[83] H. Liao, Y. Chou, Y. Wang, H. Zhang, T. Cheng, G. Liu, ChemCatChem 9 (2017) 3197-3202.
[84] B. Han, L. Zhao, Y. Song, Z. Zhao, D. Yang, R. Liu, G. Liu, Catal. Sci. Technol. 8 (2018) 2920-2927.
[85] Z. Zhao, C. Wang, Q. Chen, Y. Wang, R. Xiao, C. Tan, G. Liu, ChemCatChem 13 (2021) 4055–4063.
[86] S. Itsuno, S. Takahashi, ChemCatChem 9 (2017) 385-388.
[87] Y. Kawakami, A. Borissova, M.R. Chapman, G. Goltz, E. Koltsova, I. Mitrichev, A.J. Blacker, Eur. J. Org. Chem. 2019 (2019) 7499-7505.
[88] A. Zoabi, S. Omar, R. Abu-Reziq, Eur. J. Inorg. Chem. 2015 (2015) 2101-2109.
[89] M. Vasiloiu, P. Gaertner, R. Zirbs, K. Bica, Eur. J. Org. Chem. 2015 (2015) 2374-2381.
[90] H. Uchimoto, T. Tsuji, I. Kawasaki, K. Arimitsu, H. Yasui, M. Yamashita, S. Ohta, K. Nishide, Chem. Pharm. Bull. 63 (2015) 200-209.
[91] X. Liu, C. Chen, Y. Xiu, A. Chen, L. Guo, R. Zhang, J. Chen, Z. Hou, Catal. Commun. 67 (2015) 90-94.
[92] S. Denizalti, D. Mercan, B. Sen, A. G. Gokce, B. Cetinkaya, J. Organomet. Chem. 779 (2015) 62-66.
[93] Á.M. Pálvölgyi, J. Bitai, V. Zeindlhofer, C. Schröder, K. Bica, ACS Sustain. Chem. Eng. 7 (2019) 3414−3423.

[94] M. Hejazifar, A.M. Palvoelgyi, J. Bitai, O. Lanaridi, K. Bica-Schroeder, Org. Proc. Res. Dev. 23 (2019) 1841-1851.
[95] X. Li, Y. Sun, S. Wang, X. Jia, ACS Appl. Polym. Mater. 2 (2020) 1268–1275.
[96] X. Wang, L. Xu, F. Xiong, Y. Wu, F. Chen, RSC Adv. 6 (2016) 37701-37709.
[97] Z. Lin, J. Li, Q. Huang, Q. Huang, Q. Wang, L. Tang, D. Gong, J. Yang, J. Zhu, J. Deng, J. Org. Chem. 80 (2015) 4419-4429.
[98] J. Li, Z. Lin, Q. Huang, Q. Wang, L. Tang, J. Zhu, J. Deng, Green Chem. 19 (2017) 5367-5370.
[99] B. He, L.-S. Zheng, P. Phansavath, V. Ratovelomanana-Vidal, ChemSusChem 12 (2019) 3032-3036.
[100] J. Li, J. Han, Z. Lin, L. Tang, Q. Huang, Q. Wang, J. Zhu, J. Deng, Tetrahedron 75 (2019) 422-428.
[101] F. Liu, P. Qu, M. Weck, Org. Lett. 24 (2022) 4099−4103.
[102] J. Lu, J. Dimroth, M. Weck, J. Am. Chem. Soc. 137 (2015) 12984-12989.
[103] M. Kuepfert, A.E. Cohen, O. Cullen, M. Weck, Chem. Eur. J. 24 (2018) 18648-18652.
[104] P. Qu, M. Kuepfert, M. Hashmi, M. Weck, J. Am. Chem. Soc. 143 (2021) 4705−4713.
[105] R. Kuwano, R. Morioka, M. Kashiwabara, N. Kameyama, Angew. Chem. Int. Ed. 51 (2012) 4136−4139.
[106] D.-S. Wang, Q.-A. Chen, S.-M. Lu, Y.-G. Zhou, Chem. Rev. 112 (2012) 2557−2590.
[107] C. Margarita, P. G. Andersson, J. Am. Chem. Soc. 139 (2017) 1346−1356.
[108] S. Kraft, K. Ryan, R. B. Kargbo, J. Am. Chem. Soc. 139 (2017) 11630−11641.
[109] T. Gensch, M. Teders, F. Glorius, J. Org. Chem. 82 (2017) 9154−9159.
[110] T. Yasukawa, R. Masuda, S. Kobayashi, Nature Catal. 2 (2019) 1088-1092.
[111] L. Tao, Y. Ren, C. Li, H. Li, X. Chen, L. Liu, Q. Yang, ACS Catal. 10 (2020) 1783-1791.
[112] R. Duque, P.J. Pogorzelec, D.J. Cole-Hamilton, Angew. Chem. Int. Ed. 52 (2013) 9805−9807.
[113] E.J. O'Neal, C.H. Lee, J. Brathwaite, K.F. Jensen, ACS Catal. 5 (2015) 2615−2622.
[114] D. Geier, P. Schmitz, J. Walkowiak, W. Leitner, G. Francio, ACS Catal. 8 (2018) 3297−3303.
[115] T. Touge, M. Kuwana, K. Komatsuki, S. Tanaka, K. Matsumu, N. Sayo, Y. Kashibuchi, T. Saito, Org. Process Res. Dev. 23 (2019) 452−461.
[116] R.M. Bullock, Science 342 (2013) 1054−1055.
[117] J.R. Ludwig, C.S. Schindler, Chem 2 (2017) 313−316.
[118] F. Agbossou-Niedercorn, C. Michon, Coord. Chem. Rev. 425 (2020) 213523-213559.

[119] J. Wen, F. Wanga, X. Zhang, Chem. Soc. Rev. 50 (2021) 3211-3237.

[120] J.A. Gladysz, Pure Appl. Chem. 73 (2001) 1319−1324.

[121] S. Hübner, J.G. de Vries, V. Farina, Adv. Synth. Catal. 358 (2016) 3−25.